Journal of Medicinal Chemistry

pubs.acs.org/jmc Article

Structural Insights into JAK2 Inhibition by Ruxolitinib, Fedratinib, and Derivatives Thereof

Ryan R. Davis, Baoli Li, Sang Y. Yun, Alice Chan, Pradeep Nareddy, Steven Gunawan, Muhammad Ayaz, Harshani R. Lawrence, Gary W. Reuther, Nicholas J. Lawrence, and Ernst Schönbrunn*

Cite This: J. Med. Chem. 2021, 64, 2228−2241 Read Online

ACCESS | Metrics & More | Article Recommendations | Supporting Information

ABSTRACT: The discovery that aberrant activity of Janus kinase 2 (JAK2) is a driver of myeloproliferative neoplasms (MPNs) has led to significant efforts to develop small molecule inhibitors for this patient population. Ruxolitinib and fedratinib have been approved for use in MPN patients, while baricitinib, an achiral analogue of ruxolitinib, has been approved for rheumatoid arthritis. However, structural information on the interaction of these therapeutics with JAK2 remains unknown. Here, we describe a new methodology for the large-scale production of JAK2 from mammalian cells, which enabled us to determine the first crystal structures of JAK2 bound to these drugs and derivatives thereof. Along with biochemical and cellular data, the results provide a comprehensive view of the shape complementarity required for chiral and achiral inhibitors to achieve highest activity, which may facilitate the development of more effective JAK2 inhibitors as therapeutics.

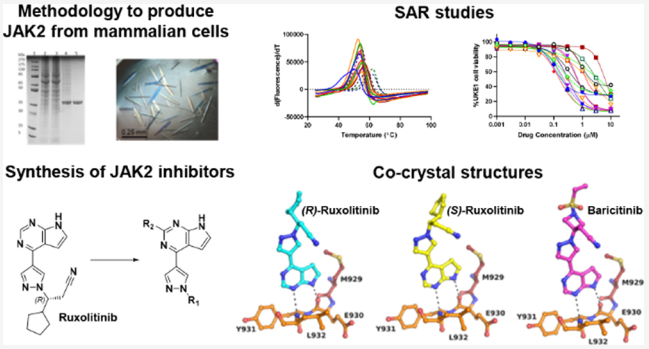

INTRODUCTION

Protein kinases have become one of the most desired classes of drug targets given their crucial roles in the regulation of cellular proliferation, survival, signaling, metabolism, and homeostasis. As a mediator of cytokine receptor activation, Janus kinase 2 (JAK2) is a cytosolic tyrosine kinase that phosphorylates signal transducer and activator of transcription proteins (STATs) resulting in SH2-domain mediated dimerization and STAT activation. STATs govern many processes including cell proliferation, differentiation, and immunological responses vital for cell survival.[1] The JAK/STAT pathway has been listed as one of the 12 core cancer pathways demonstrating the importance of proper JAK2 regulation to maintain a normal cell function.[1] JAK2 is a multidomain protein (Figure S1), which undergoes *trans*-autophosphorylation on the activation loop of the kinase domain (KD) involving residues Tyr1007 and Tyr1008. The purpose of this phosphorylation is not fully known but is thought to aid in the recruitment and phosphorylation of STATs.[2] Type 1 inhibitors have been shown to bind to the adenosine triphosphate (ATP) binding site of the active conformation of JAK2, but inhibition paradoxically leads to accumulation of phosphorylated residues on the activation loop with increasing inhibitor concentration.[3,4] This phenomenon has been attributed to the protection of activation loop phosphotyrosines from phosphatases.[5,6] Higher levels of phosphorylated Tyr1007/1008, and therefore higher levels of constitutively active JAK2, have also been shown to be caused by a single hyperactivating point mutation, V617F, found in the pseudokinase domain (PKD) of JAK2.[7]

Constitutively active JAK2 has been identified in several types of cancers including breast cancer, lymphomas, and myeloid malignancies.[3,8−10] The V617F mutation is the most commonly identified mutation found in myeloproliferative neoplasms (MPNs), in more than 95% of polycythemia vera patients and in more than 50% of all thrombocythemia and primary myelofibrosis cases.[8,11] The Food and Drug Administration (FDA) approved the pyrrolopyrimidine JAK2 inhibitor ruxolitinib in 2011 and the dianilinopyrimidine inhibitor fedratinib in 2019 for treating myelofibrosis.[12−14] Baricitinib, an achiral analogue of ruxolitinib, was approved for rheumatoid arthritis in 2018.[15] JAK2 inhibitors for MPN provide quality of life improvements but little efficacy at antagonizing the natural course of disease. To date, no crystal structure of ruxolitinib has been reported with any of the JAK family proteins, making ruxolitinib the oldest FDA-approved kinase inhibitor without a cocrystal structure with its target

Received: November 17, 2020
Published: February 11, 2021

https://dx.doi.org/10.1021/acs.jmedchem.0c01952
J. Med. Chem. 2021, 64, 2228−2241

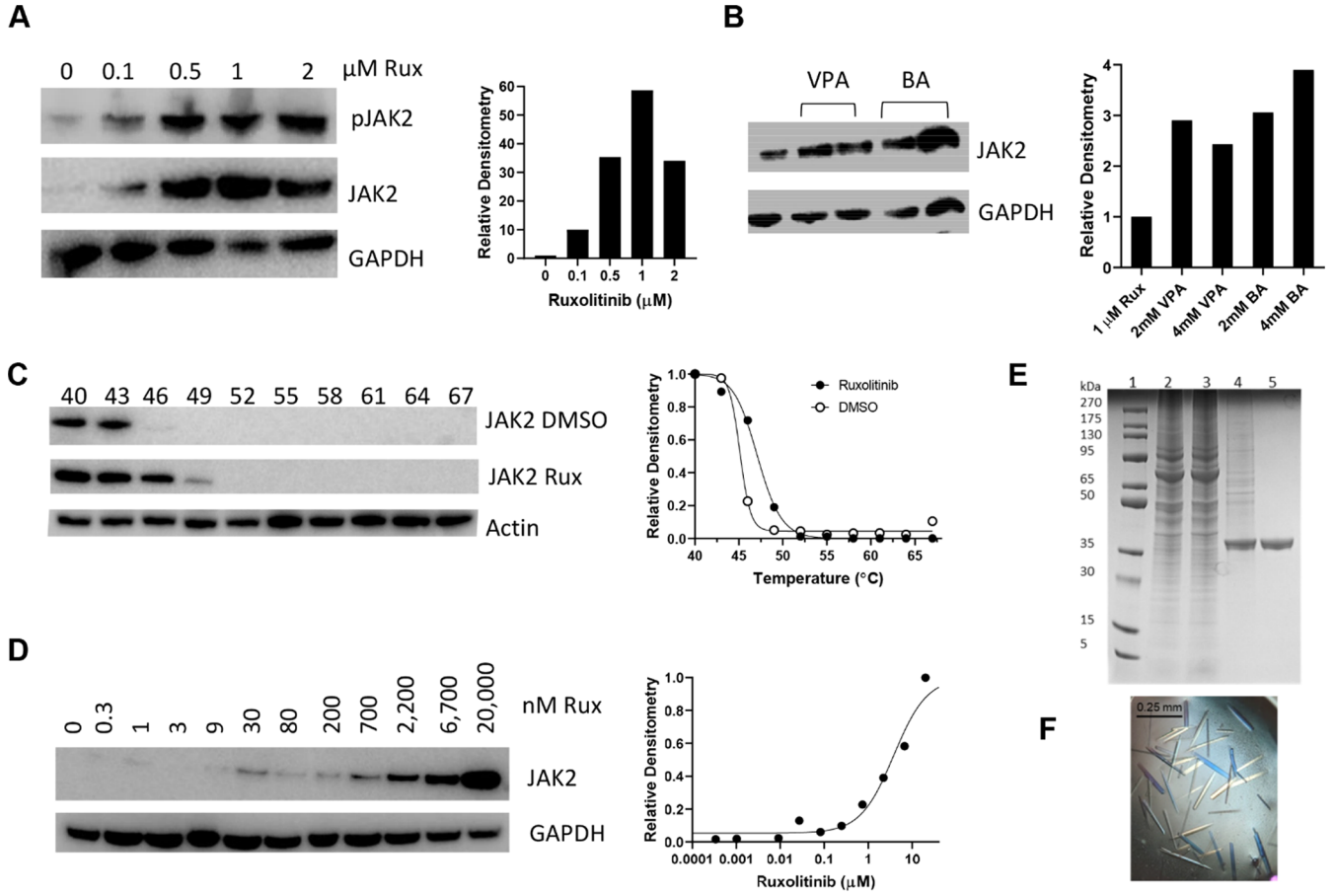

Figure 1. Ruxolitinib enhances the expression and purification of crystallization-grade JAK2 KD. (A) Expi293F cells were transiently transfected with wild-type JAK2 KD. Cells were treated with increasing concentrations of ruxolitinib during the 24-hour transfection. Cell lysates were subjected to immunoblotting to detect phosphorylated and unphosphorylated JAK2 KD along with the loading control GAPDH. Densitometry of the western blot is depicted as a bar graph. (B) Same as (A) except 2 mM and 4 mM butyric acid (BA) or valproic acid (VPA) were added to cells with 1 μM ruxolitinib. (C) Expi293F cells were transiently transfected with JAK2 KD +/− 1 μM ruxolitinib and analyzed by CETSA. Cells were incubated at the indicated temperatures for 3 min, and lysates were probed for JAK2 KD and the loading control actin. The graph shows the densitometry values relative to the loading control as a function of temperature. Data were fit to a four-parameter Hill equation, yielding EC_{50} values of 45 and 47 °C for JAK2 KD expressed in the absence and presence of ruxolitinib, respectively. (D) Cells were grown as in (C) for ITDR against ruxolitinib at 47 °C for 3 min, and cell lysates were probed for JAK2 and GAPDH. The corresponding densitometry values were fit to a four-parameter Hill equation yielding EC_{50} = 3.8 μM. (E) SDS-PAGE of typical purification of JAK2 KD from 1 L of Expi293F cell culture grown in the presence of 1 μM ruxolitinib and 4 mM BA for 24 h. Lane 1 GenScript broad range ladder, Lane 2 soluble lysate, Lane 3 GE HisTrap flow-through, Lane 4 GE HisTrap elution peak, and Lane 5 GE S75 elution peak. (F) Photograph of X-ray-grade crystals grown from thus purified JAK2 KD.

protein.[16,17] Likewise, structural information on the interaction of JAK2 with fedratinib and baricitinib remains unknown. Knowledge of these structures, however, is required for the development of more efficacious drugs to specifically target aberrant JAK2. Here, we report the first crystal structures of ruxolitinib, fedratinib, and baricitinib along with derivatives bound to the JAK2 KD. We introduce a new methodology to efficiently produce crystallization-grade JAK2 KD from mammalian cells, which enabled efficient structure−activity relationship (SAR) studies with inhibitors of different chemical scaffolds. A total of 14 high-resolution crystal structures were determined of JAK2 liganded with known and novel inhibitors. The data sets detail the requirements of small molecule inhibitors for shape complementarity with the ATP site of JAK2 and provide a structural basis for the stereoselective discrimination of enantiomers of ruxolitinib and derivatives thereof.

RESULTS

Ruxolitinib Significantly Increases the Stability of JAK2 KD Overexpressed in Expi293F Cells. Previously, JAK2 KD had been predominantly purified from insect cells; however, this process takes several weeks to generate and amplify the baculovirus to produce large enough quantities of purified protein. Upon transient expression of JAK2 KD in Expi293F cells, the presence of ruxolitinib during the transfection increased the levels of phosphorylated JAK2 (pY1007), as previously reported,[3] as well the overall amount of JAK2 KD in a concentration-dependent manner (Figure 1A). Protein levels of recombinant JAK2 KD from Expi293F cells were approximately 60-fold higher with 1 μM ruxolitinib compared to untreated cells. Additionally, by including histone deacetylase (HDAC) inhibitors, valproic acid or butyric acid, during expression alongside ruxolitinib, JAK2 KD levels increased fourfold over that of ruxolitinib alone (Figure 1B).

https://dx.doi.org/10.1021/acs.jmedchem.0c01952
J. Med. Chem. 2021, 64, 2228−2241

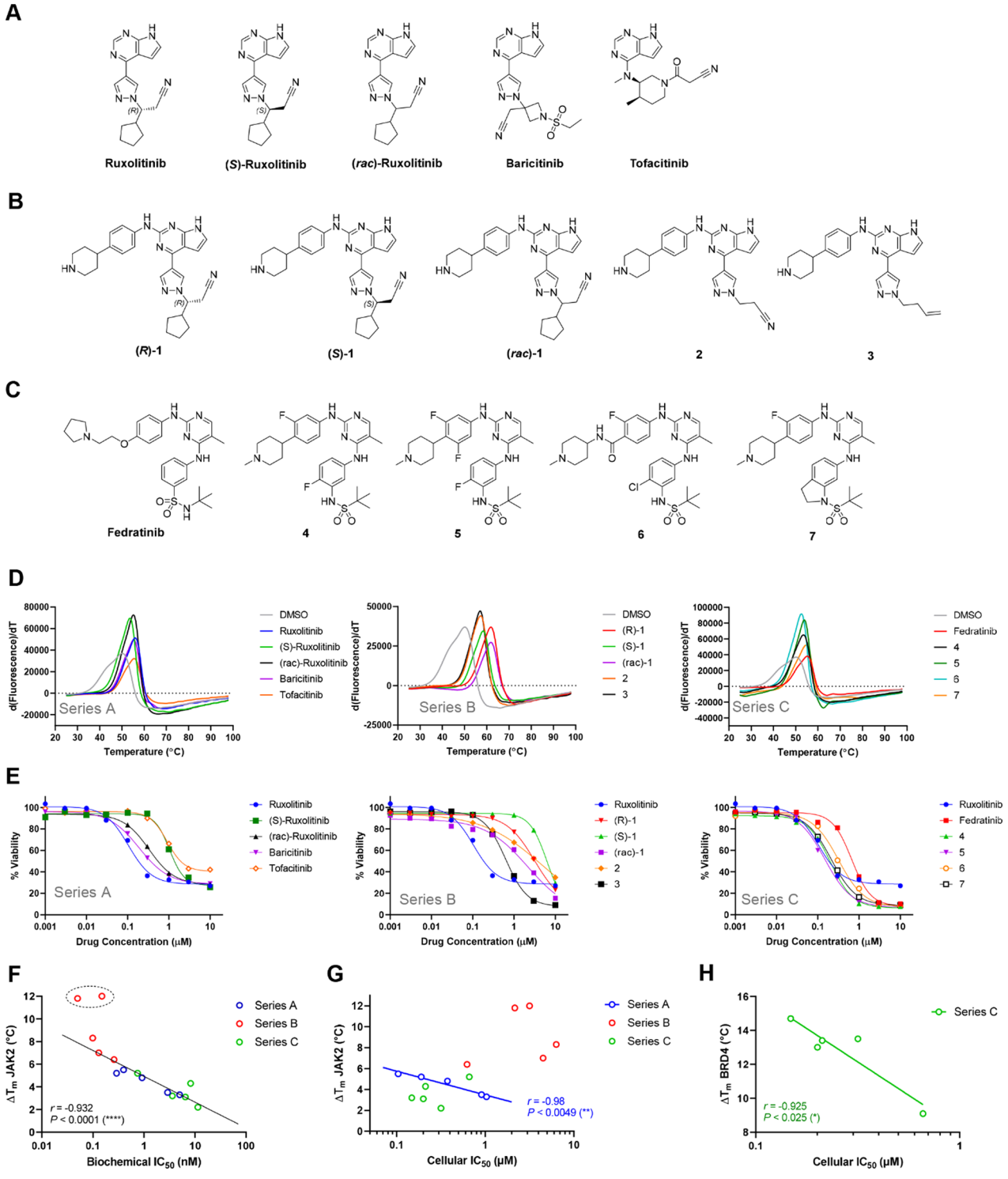

Figure 2. Purified JAK2 KD from Expi293 cells is suitable for SAR studies by DSF. Three series of JAK2 inhibitors were subjected to SAR studies: (A) Ruxolitinib stereoisomers and FDA-approved derivatives, (B) piperidine−phenylamine analogues of ruxolitinib, and (C) fedratinib and derived dual JAK2−BRD4 inhibitors. (D) DSF derivative plots of JAK2 KD in the absence (DMSO) and presence of 100 μM inhibitor. (E) Viability of UKE-1 cells in response to increasing inhibitor concentration. (F) DSF and biochemical enzyme inhibition data correlate significantly. (G) Analysis of DSF and UKE-1 cell growth inhibition data shows high correlation for series A, but not for series B and C. Series B likely suffers from poor cell permeability. (H) For series C, cell inhibition data correlate significantly with the binding potential for BRD4-1, suggesting a predominant activity through inhibition of BRD4.

Next, we investigated the thermostability of JAK2 KD upon transient expression in the presence of ruxolitinib using a cellular thermal shift assay (CETSA)[18] and isothermal dose response (ITDR). At 1 μM concentration, ruxolitinib elevated the cellular thermostability of JAK2 KD by 2 °C, from 45 to 47 °C (Figure 1C). At 47 °C, the amount of expressed JAK2 KD increased in dose-response with ruxolitinib (EC_{50} = 3.8 μM) (Figure 1D). Expression in the absence of ruxolitinib yielded

https://dx.doi.org/10.1021/acs.jmedchem.0c01952
J. Med. Chem. 2021, 64, 2228−2241

very little soluble protein and purity could not be achieved above 50% (data not shown). Adding ruxolitinib to cells during transfection resulted in significantly more protein, which could be purified to homogeneity using Ni-affinity and size-exclusion chromatography with yields of 3 mg/L culture (Figure 1E). Purified JAK2 KD yielded X-ray grade crystals within 24 h (Figure 1F).

SAR Studies of Diverse Small Molecule JAK2 Inhibitors. To assess the suitability of purified JAK2 KD for SAR studies for drug development campaigns, three series of JAK2 inhibitors (Figure 2A-C) were subjected to binding studies by differential scanning fluorimetry (DSF). Series A consists of ruxolitinib enantiomers and FDA-approved derivatives baricitinib and tofacitinib, while series B consists of piperidine−aniline analogues of ruxolitinib. Series C comprises the FDA-approved JAK2 inhibitor fedratinib and other diaminopyrimidines, which were further developed as dual JAK2−BRD4 inhibitors from early lead compounds.[19] The melting temperature of JAK2 in the absence of an inhibitor was 50 °C, and thermal shifts in the presence of a 100 μM inhibitor ranged from 3.3 to 5.5 °C for series A, 6.4 to 12 °C for series B, and 2.2 to 5.2 °C for series C (Figure 2D and Table 1).

Table 1. Binding and Inhibitory Potential of Investigated JAK2 Inhibitors

series	compound ID	binding potential[a]	biochemical inhibition[b]	UKE-1 cell growth inhibition[c]
		ΔT_m (°C)	IC_{50} (nM)	IC_{50} (μM)
A	Ruxolitinib	5.5 ± 0.06	0.40 ± 0.005	0.1 ± 0.02
	(*S*)-Ruxolitinib	3.3 ± 0.04	5.0 ± 0.1	1.04 ± 0.09
	(rac)-Ruxolitinib	4.8 ± 0.05	0.92 ± 0.06	0.38 ± 0.08
	Baricitinib	5.2 ± 0.08	0.29 ± 0.13	0.19 ± 0.03
	Tofacitinib	3.5 ± 0.08	2.9 ± 0.39	0.91 ± 0.1
B	(*R*)-1	12 ± 0.02	0.15 ± 0.03	3.2 ± 0.76
	(*S*)-1	8.3 ± 0.08	0.099 ± 0.02	6.3 ± 5.4
	(rac)-1	11.8 ± 0.05	< 0.05	2.2 ± 1.9
	2	7 ± 0.03	0.13 ± 0.048	4.5 ± 5.9
	3	6.4 ± 0.04	0.26 ± 0.04	0.62 ± 0.04
C	Fedratinib	5.2 ± 0.07	0.75 ± 0.39	0.66 ± 0.06
	4	3.1 ± 0.09	6.5 ± 3.5	0.2 ± 0.02
	5	3.2 ± 0.04	8.2 ± 5.7	0.15 ± 0.01
	6	2.2 ± 0.06	11.4 ± 0.87	0.32 ± 0.02
	7	4.3 ± 0.05	3.6 + 1.1	0.21 ± 0.02

[a]Standard deviation (SD) from two DSF data sets, each performed in quadruplicate. [b]SD from two data sets of radiometric assay by Reaction Biology. [c]Standard error of the mean (SEM) for data from three experiments, each performed in hexaplicate.

To evaluate if the thermal shifts reflect the inhibitory activity against JAK2 in cells, compounds were characterized for growth inhibitory activity of UKE-1 cells, which are driven by V617F mutant JAK2 (Figure 2E).[20] The resulting IC_{50} values ranged from 0.1 to 1.0 μM for series A, 0.6 to 6.3 μM for series B, and 0.15 to 0.66 μM for series C. Additionally, compounds were characterized for inhibition of the enzymatic JAK2 activity using a radiometric assay by Reaction Biology Corp., with IC_{50} values ranging from 0.29 to 5.0 nM for series A, 0.05 to 0.26 nM for series B, and 0.75 to 11.4 nM for series C (Table 1). Statistical significance of the data sets was evaluated using Pearson's correlation analyses (Figure 2F-H). Thermal shifts showed excellent correlation with enzymatic inhibition values across all compounds, except for (*R*)-**1** and *rac*-**1** of series B, the high inhibitory activity of which likely exceeded the sensitivity of the radiometric assay applied (IC_{50} < 0.15 nM) (Figure 2F). By contrast, only series A showed significant correlation with the cellular inhibition data (Figure 2G). Series B probably suffered from poor cell permeability, while series C showed a higher cell growth inhibitory activity than expected from JAK2 inhibition alone. The increased cellular activity of series C is likely caused by their dual activity against JAK2 and BRD4 as UKE-1 cells are highly sensitive to the inhibition of BRD4.[19] The thermal shifts exerted by these compounds toward BRD4 correlated significantly with the inhibitory activity against UKE-1 cell growth (Figure 2H).

Structural Basis of JAK2 Inhibition by Ruxolitinib and Baricitinib. Structural information on the JAK2−ruxolitinib complex was previously limited to molecular dynamics simulations[16] or predictions based on the known structures of c-SRC with ruxolitinib[21] and of JAK2 with tofacitinib.[22] Crystals of JAK2 KD grown in the absence of an added inhibitor (Figure 1F) showed that ruxolitinib was still bound to protein despite ∼100,000-fold dilution throughout the purification process, reflecting the high binding affinity of ruxolitinib to JAK2 KD. However, bound ruxolitinib could be readily displaced by other inhibitors through in-diffusion of crystals with 1 mM inhibitor for 72 h prior to data collection. Ruxolitinib was housed deep inside the ATP site, anchored through H-bonding interactions between the pyrrolopyrimidine moiety and main chain atoms of Glu930 and Leu932 of the hinge region (Figure 3A-D).

The inhibitor was held in place through several van der Waals (vdW) hydrophobic interactions with surrounding residues, including the P-loop (Leu855 and Gly856) and the DFG motif (Asp994). The binding pose of ruxolitinib in JAK2 agrees with molecular docking predictions[16] but significantly differs from that observed in the crystal structure of c-SRC (Figure 3E).[21] In SRC, ruxolitinib is rotated ∼180° relative to the hinge region, likely caused by repulsion and/or steric hindrance with the gatekeeper residue Thr338. In JAK2, the hydrophobic and flexible gatekeeper residue Met929 accommodates ruxolitinib through multiple vdW interactions. Accordingly, ruxolitinib inhibitory activity is three orders of magnitudes higher for JAK2 over SRC.[21] To confirm the pyrrolopyrimidine binding mode of ruxolitinib in JAK2, a cocrystal structure was determined with baricitinib showing almost identical positioning of the two inhibitors in the ATP site (Figure 3F).

Stereoselective Discrimination of Ruxolitinib and Aniline Derivatives by JAK2. The high diffraction power of the JAK2 KD crystals prompted us to evaluate the SAR of enantiomers of ruxolitinib and analogues thereof. The (*S*)-isomer of ruxolitinib is ∼10-fold less active against JAK2 than the (*R*)-isomer (Table 1). The cocrystal structure revealed that (*S*)-ruxolitinib adopts a binding pose similar to (*R*)-ruxolitinib (Figure 4A) and achieves shape complementarity with the ATP site through ∼180° rotation about the chiral center (Figure 4B). Using the racemic mixture of ruxolitinib, (*rac*)-ruxolitinib, the resulting cocrystal structure exclusively revealed the (*R*)-isomer bound (Figure 4C). Likewise, the (*R*)- and (*S*)-enantiomers of aniline derivatives of ruxolitinib, (*R*)-**1** and (*S*)-**1**, assumed the same orientation for the cyclopentyl and propionitrile moieties in the ATP site (Figure 4D-F). Furthermore, the racemic mixture (*rac*-**1**) showed only the

https://dx.doi.org/10.1021/acs.jmedchem.0c01952
J. Med. Chem. 2021, 64, 2228−2241

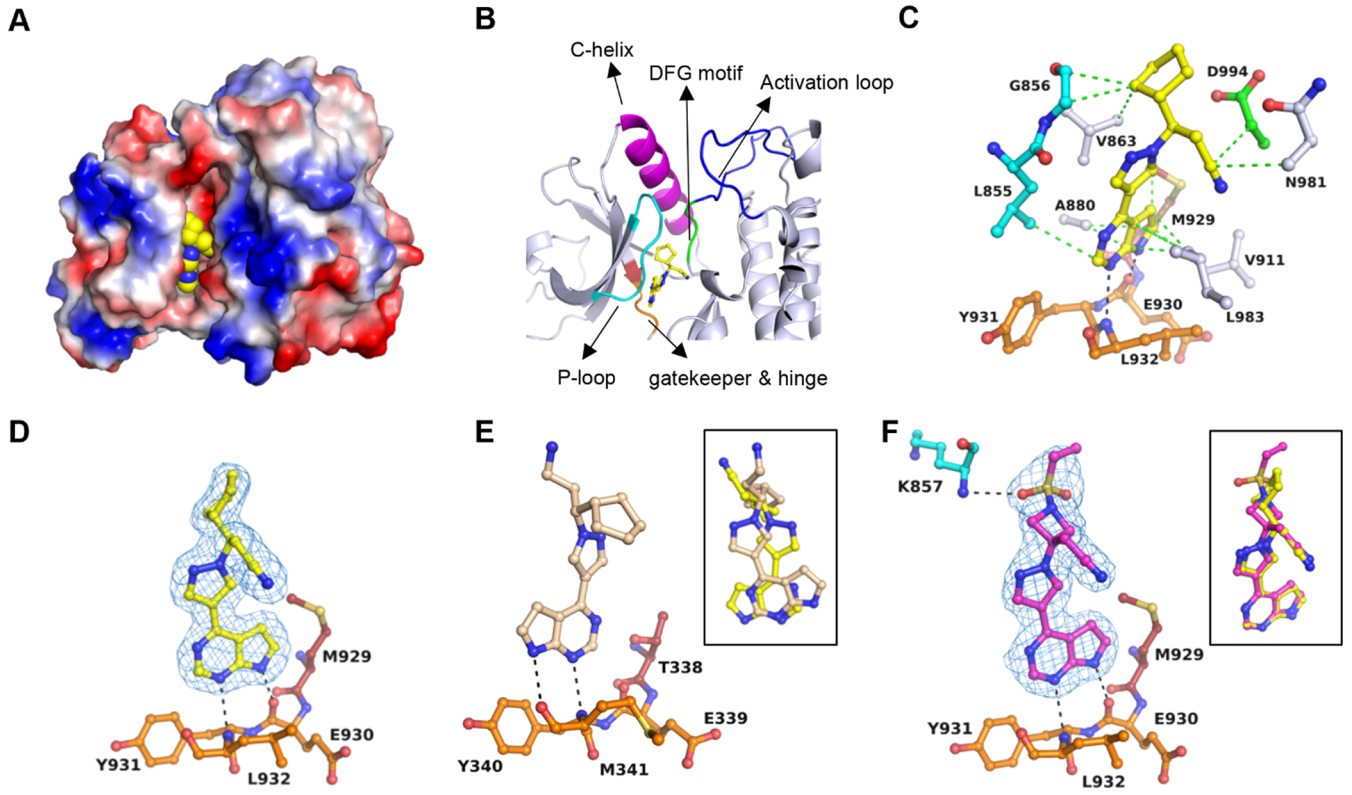

Figure 3. Structural basis of ruxolitinib interaction with JAK2. Cocrystal structure of JAK2 KD liganded with ruxolitinib determined at 1.9 Å resolution (PDB 6VGL). (A) Electrostatic surface potential of the JAK2−ruxolitinib complex. The inhibitor is shown as yellow spheres. (B) Positioning of ruxolitinib in the ATP site. The hinge region is shown in orange, gatekeeper residue in red, DFG motif in green, P-loop in cyan, C-helix in magenta, and other residues in grey. (C) Binding interactions of ruxolitinib in the ATP site. Potential H-bonding and hydrophobic vdW interactions are indicated as black and green dotted lines, respectively. (D) 2Fo−Fc electron density map (1σ) of bound ruxolitinib at 1.9 Å resolution. (E) Binding pose of ruxolitinib (beige) in c-SRC (PDB 4U5J) and upon superposition with ruxolitinib in JAK2 (yellow). (F) 1.9 Å resolution cocrystal structure of JAK2 with baricitinib (magenta, PDB 6VN8) and superposition with ruxolitinib (yellow).

(*R*)-isomer bound (Figure 4G). The data demonstrate that JAK2 discriminates between the (*R*)- and (*S*)-stereoisomers of ruxolitinib and derivatives by preferentially interacting with the (*R*)-isomer. Ruxolitinib derivatives devoid of a chiral center and the cyclopentyl group (**2** and **3**) exhibited the same preference of the respective propionitrile and butenyl moieties for positioning in the subpocket that accommodates the propionitrile of ruxolitinib (Figure 4H,I). Notably, the aniline derivatives interacted in the ATP site through an additional H-bond with the hinge region (Figure 4D-I), which explains the substantial increase in the JAK2 inhibitory activity of series B over ruxolitinib and series A (Table 1).

Structural Basis of JAK2 Inhibition by Diaminopyrimidines. To further probe the ATP site, cocrystal structures were determined with dianilinopyrimidine-containing inhibitors of series C. All inhibitors interacted with the hinge region similarly to the aniline derivatives of ruxolitinib (Figure 5).

However, the lack of a pyrrolo moiety allows only for the establishment of H-bonds with the main chain atoms of Leu932, but not with Glu930. This is reflected by the 10-fold reduced biochemical potency of inhibitors of series C against JAK2 (Table 1). Reversal of the sulfonamide moiety and addition of fluorine (**4**), which are beneficial for binding to the acetyl-lysine binding site of BRD4,[19] slightly tilted the aniline ring such that the *tert*-butyl moiety moves away from Val863 and positions close to the carboxyl group of Asp994 of the DFG motif (Figure 5B). Although the reversed sulfonamide forms potential H-bonds with the side chain of Asn981, the unfavorably close distance between the hydrophobic *tert*-butyl and Asp994 may contribute to the observed slight reduction in inhibitory activity of **4** and related compounds **5** and **6** (Figure 5C,D). Constraining the sulfonamide moiety using an indoline moiety (**7**) was well tolerated (Figure 5E) and showed the highest inhibitory activity against JAK2 across series C (Table 1).

DISCUSSION AND CONCLUSIONS

JAK2 presents challenges for structural studies as it is not stable upon recombinant overexpression, and typical protein purification requires over 10 L of insect cultures from bioreactors to obtain a few milligrams of crystallization-grade protein.[23−26] Recombinant overexpression of JAK2 KD using mammalian Expi293F cells requires only 24 h of growth post-transfection, and 1 L of culture is sufficient to purify milligram quantities of crystallization-grade protein for biochemical and structural studies. This was achieved using ruxolitinib during expression, which significantly enhanced protein stability and purification yields and enabled the first crystal structures of JAK2 to be determined from protein expressed in mammalian cells. The crystal structure data suggest that ruxolitinib improves the thermostability of JAK2 by decreasing flexible regions and forming a more rigid structure with well-defined activation and P-loops. Notably, ruxolitinib did not affect the proliferation of Expi293F or HEK293 cells even at 10 μM after 72 h.[19] This strategy provided faster, more efficient, and cost-effective production of recombinant JAK2 and may be

https://dx.doi.org/10.1021/acs.jmedchem.0c01952
J. Med. Chem. 2021, 64, 2228−2241

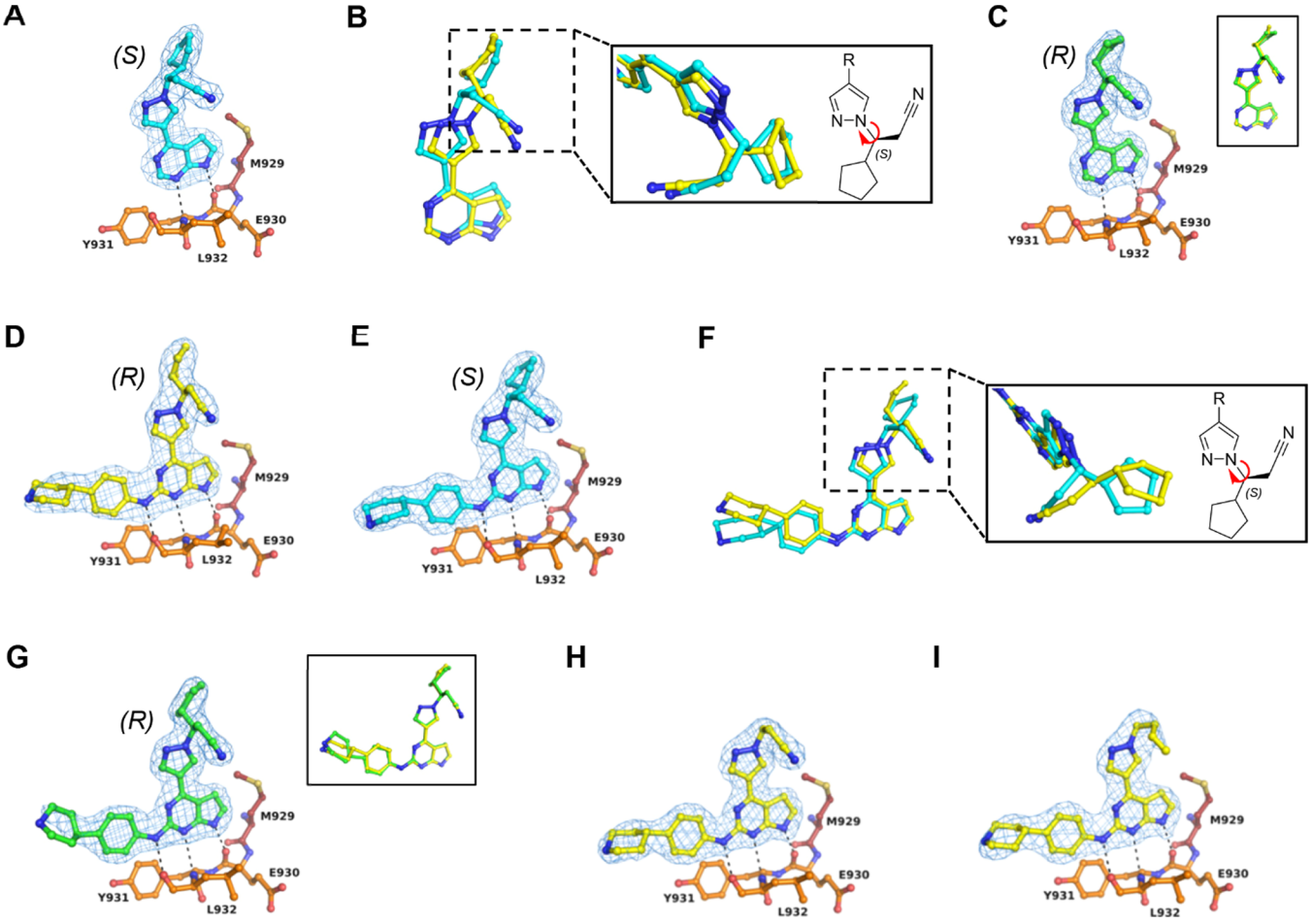

Figure 4. JAK2 discriminates between the (*R*)- and (*S*)-stereoisomers of ruxolitinib and derivatives thereof. Distinct stereoisomers and the enantiomeric mixture of ruxolitinib and derivatives were subjected to crystallographic studies with JAK2 KD. (A) Cocrystal structure of (*S*)-ruxolitinib (PDB 6VSN). (B) Superposition of the (*R*)- and (*S*)-isomers of ruxolitinib (yellow and cyan, respectively) reveals that (*S*)-ruxolitinib adopts shape complementarity with the ATP site through ∼180° rotation about the stereocenter. (C) Cocrystal structure obtained with the racemic mixture of ruxolitinib, (*rac*)-ruxolitinib (PDB 6VNK) reveals only the (*R*)-isomer bound (green). The inset shows the superposition of (*rac*)-ruxolitinib with ruxolitinib. (D) Cocrystal structure showing the H-bonding interactions of (*R*)-**1** (yellow, PDB 6VNC) with the hinge region. (E) Same as (D) for the (*S*)-**1** (cyan, PDB 6VNB). (F) Superposition of (*R*)-**1** and (*S*)-**1** reveals the same adaptation as for ruxolitinib (B). (G) Cocrystal structure obtained with (*rac*)-**1** (green, PDB 6VS3) shows only the (*R*)-isomer bound. The inset shows the superposition of (*rac*)-**1** with (*R*)-**1** (yellow). (H) Cocrystal structure with derivative **2** devoid of a stereocenter (PDB 6VNJ) reveals the same binding pose and inhibitor conformation as (*R*)-**1**. (I) Same as (H) for derivative **3** (PDB 6VNM). The blue mesh is the 2Fo−Fc electron density of ligand contoured at 1σ. The electron density maps upon refinement omitting the ligand are shown in Figure S2.

applicable to other difficult to overexpress kinases provided that the inhibitor is specific, potent, and nonlethal over the timeframe of expression.

Robust crystallization conditions and ease of in-diffusion of inhibitors resulted in 14 novel cocrystal structures of JAK2 liganded with various inhibitors of three chemical scaffolds. Along with binding and inhibition data, this information provides a comprehensive view of the ATP site and the shape complementarity required for small molecules to achieve highest inhibitory activity. The (*R*)- and (*S*)-stereoisomers of ruxolitinib and aniline derivatives thereof were thoroughly characterized for their binding potential and inhibitory activity against cancer cells driven by constitutively active V617F JAK2. While (*S*)-ruxolitinib is a formidable inhibitor of JAK2 (IC_{50} = 5 nM), the (*R*)-isomer exerted a > 10-fold higher activity with respect to binding and cell kill potential. Cocrystal structures obtained with the isolated isomers along with racemic mixtures demonstrate that JAK2 discriminates against the (*S*)-configuration. The (*S*)-isomer mimics the conformation of the preferred (*R*)-isomer through rotation about the chiral center, but the resulting binding pose is less compatible with the ATP site. Notably, the achiral analogue baricitinib adopts a conformation almost identical to that of ruxolitinib, which is reflected in the similar values obtained for binding, enzymatic, and cellular activities of these FDA-approved inhibitors.

Piperidine−aniline derivatives of both (*R*)- and (*S*)-ruxolitinib showed greatly enhanced binding and inhibitory potential toward JAK2; the picomolar activities could not be resolved by the steady-state assays employed here. This substantial increase in inhibitory activity is attributed to an additional H-bond established with the hinge region. Although these compounds suffer from poor cell penetration as indicated by a significant loss of the cell inhibitory activity, solubilizing groups other than piperidine may alleviate this drawback. Diaminopyrimidine inhibitors of JAK2, including fedratinib, mimic the binding pose of aniline derivatives of ruxolitinib. However, they lack the potential to establish an H-bond with

https://dx.doi.org/10.1021/acs.jmedchem.0c01952
J. Med. Chem. 2021, 64, 2228−2241

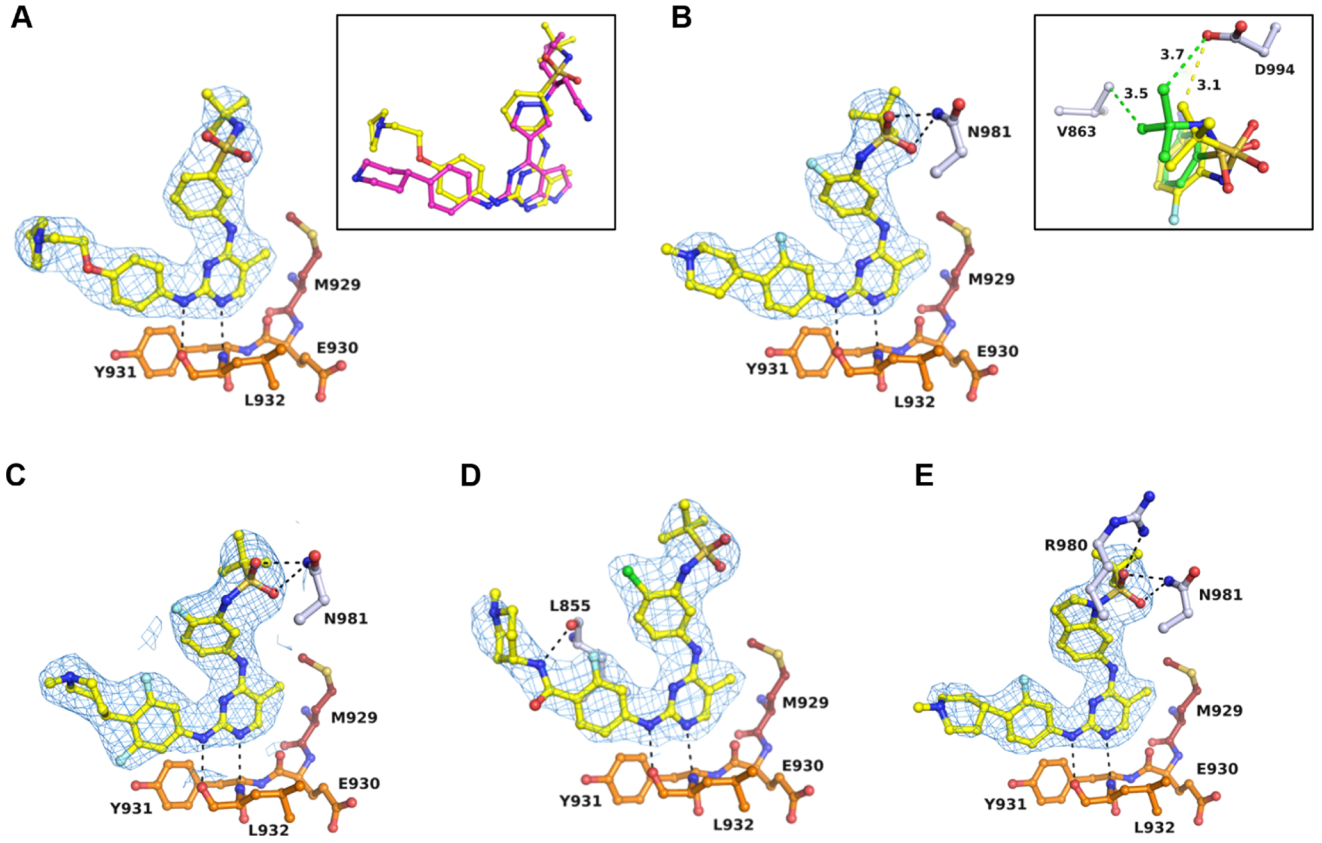

Figure 5. Diaminopyrimidine inhibitors mimic the binding pose of ruxolitinib−aniline derivatives. (A) Cocrystal structure of JAK2 with fedratinib (PDB 6VNE). The inset shows the superposition of fedratinib (yellow) with (*R*)-**1** (magenta). (B) Cocrystal structure with **4** (PDB 6VNG). The inset shows the superposition of **4** (yellow) with fedratinib (green). (C) Cocrystal structure with **5** (PDB 6VNH). (D) Cocrystal structure with **6** (PDB 6VNL). (E) Cocrystal structure with **7** (PDB 6VNF).

Glu930 of the hinge region, which is reflected by the reduced but still formidable inhibitory activities (IC_{50} between 0.75 and 11.4 nM). These compounds also inhibit BET bromodomains to varying degrees and appear to exert a strong cell growth inhibitory activity by predominantly targeting BRD4. Previously, structural modeling, binding, and enzymatic assays using full-length JAK2 expressed in insect cells showed high affinity of fedratinib for the substrate-binding site.[3] The cocrystal structure of JAK2 KD with fedratinib (or any other compound studied herein) showed that the inhibitor bound exclusively to the ATP site. It is conceivable that fedratinib interaction with the substrate-binding site occurs in the full-length enzyme, but not in the isolated KD. Combined, our findings may help the iterative drug design process for developing JAK2 inhibitors with increased efficacy to combat cancers caused by this enzyme.

EXPERIMENTAL SECTION

Compounds and Reagents. Reagents for biochemical and crystallographic experiments were purchased from Fisher Scientific and Hampton Research unless otherwise indicated. Ruxolitinib (phosphate) was purchased from LC Laboratories (R-6688, >99%), tofacitinib (citrate) from MedChemExpress (HY-40354A, 99.1%), baricitinib (free base) from Combi-Blocks (QJ-1094, 98%), and fedratinib from MedChemExpress (HY-10409, 99.9%). The following antibodies were used for immunoblotting: His-HRP (ProteinTech, HRP-66005, 1:5000), pJAK2 (Y1007/1008) (Cell Signaling, 3771, 1:1000), actin (Sigma, A5441, 1:1000), GAPDH-HRP (ProteinTech, HRP-60004, 1:10,000), and anti-mouse-HRP IgG (Jackson ImmunoResearch, 115-035-003, 1:2000).

General Synthetic Methods. All reagents were purchased from commercial suppliers and used without further purification. ^{1}H nuclear magnetic resonance (NMR) spectra were recorded using a Bruker 500 MHz spectrometer with $CDCl_3$, CD_3OD, or DMSO-d_6 as the solvent. ^{13}C NMR spectra were recorded at 125 MHz. All coupling constants were measured in Hertz (Hz), and the chemical shifts (δ_H and δ_C) were quoted in parts per million (ppm) relative to TMS (δ 0), which was used as the internal standard. High-resolution mass spectroscopy was carried out using an Agilent 6210 LC/MS (ESI-TOF). High-performance liquid chromatography−mass spectrometry (HPLC-MS) analysis was performed using an Agilent 6120 single-quadrupole 1220 LC/MS equipped with a Zorbax SB-C18 column (4.6 × 50 mm, 1.8 μm). The purity of final compounds that underwent biological assessment was >95% as measured by HPLC-MS. Thin-layer chromatography (TLC) was performed using silica gel 60 F254 plates (Fisher), with observation under UV when necessary. Anhydrous solvents (acetonitrile, dimethylformamide, ethanol, isopropanol, methanol, and tetrahydrofuran) were used as purchased from Aldrich. Burdick and Jackson HPLC-grade solvents (methanol, acetonitrile, and water) were purchased from VWR for HPLC and high-resolution mass analysis. HPLC-grade trifluoroacetic acid (TFA) was purchased from Fisher. Compound synthesis and characterization are detailed in the Supporting Information.

Compound Synthesis and Characterization. *Pyrrolopyrimidine Inhibitors of JAK2.* (*S*)-Ruxolitinib was prepared by a novel resolution of pyrazole-containing carboxylic acid **9** (from conjugate addition of 4-bromo-1*H*-pyrazole and ester hydrolysis of **8**[27]) as shown in Scheme S1. Reaction of **9** with the Evans oxazolidinone provided the diastereoisomeric oxazolidinones (4*R*,3*R*)-**10** and (4*R*,3*S*)-**10**, which were easily separated to homogeneity by flash chromatography on a silica gel. The faster-running fraction was identified as (4*R*,3*S*)-**10** by correlation to the enantiomer of clinically

https://dx.doi.org/10.1021/acs.jmedchem.0c01952
J. Med. Chem. 2021, 64, 2228−2241

used (*R*)-ruxolitinib using the synthetic route described in a reported patent.[27] Treatment of (4*R*,3*S*)-**10** with ammonium hydroxide[28] gave the primary amide **11**, which upon dehydration with phosphorus pentoxide gave the nitrile **12**. Formation of the boronate ester **13** followed by a Suzuki reaction with 4-bromo-7*H*-pyrrolo[2,3-*d*]-pyrimidine provided (*S*)-ruxolitinib. The enantiomeric excess of (*S*)-ruxolitinib was determined to be >99.99% by chiral HPLC (Figure S3). A sample of (*rac*)-ruxolitinib was prepared from *rac*-**13** in the same way. The synthesis of the ruxolitinib analogues (*R*)- and (*S*)-**1** is shown in Schemes S1,S2. 2-Chloro-ruxolitinib (**14**) was prepared by Suzuki coupling of **13** with 2,4-dichloropyrrolopyrimidine (Scheme S1). Substitution of the chlorine atom with the anilinopyrimidine substituent required protection of the pyrrole NH group. Thereby, Buchwald−Hartwig amination of the boc-protected pyrrolopyrimidine **15** gave **16** bearing anilinopiperidine at the 2-position of the pyrimidine ring. Finally, removal of the protecting groups gave the desired (*S*)-**1** bearing the required piperidine group oriented toward the solvent-accessible region. Again, a chiral HPLC analysis indicated that the enantiomeric excess of (*S*)-**1** was >99.99% (as determined by the e.e. of its *bis*-boc protected precursor (*S*)-**16**, Figure S4). The enantiomer (*R*)-**1** was prepared in the same way using the diastereoisomer (4*R*,3*R*)-**10** (Scheme S2). In this case, the enantiomeric excess of (*R*)-**1** was 98.6% (as determined by the e.e. of its *bis*-boc protected precursor (*R*)-**22**. Ruxolitinib derivatives lacking the cyclopentyl group have been shown to retain potent JAK2 inhibitory activity.[29,30] Thus, piperidine **2**, incorporating the propionitrile-substituted pyrazole, was prepared in a similar way by Suzuki reaction of addition of 2,4-dichloropyrrolopyrimidine and the boronic ester **27** (from acrylonitrile and 4-pyrazoleboronic pinacolate[31]) to give the nitrile **28** (Scheme S3). A similar sequence of Buchwald−Hartwig amination of the boc-protected 2-chloropyrrolopyrimidine **29** followed by deprotection of **30** provided piperidine **2**. The piperidine **3**, bearing a butenyl-substituted pyrazole group, was prepared using the same methods used to prepare piperidine **2** (Scheme S4).

*Methyl 3-(4-Bromo-1H-Pyrazol-1-yl)-3-Cyclopentylpropanoate (**8**).* This compound was prepared according to the reported method.[27] To a solution of 3-cyclopentyl methacrylate (4.56 g, 29.58 mol, 1.0 eq) in anhydrous acetonitrile (100 mL), 4-bromopyrazole (4.77 g, 32.49 mol, 1.1 eq) and 1,8-diazabicyclo[5.4.0]undec-7-ene (DBU) (6.63 mL, 44.37 mol, 1.5 eq) were added. The reaction mixture was stirred overnight at room temperature. The mixture was concentrated under a reduced pressure and the residue was dissolved in ethyl acetate (EtOAc, 500 mL), 1 N HCl was added to adjust the pH value to 3 or 4, and then washed with water (100 mL) and brine (100 mL). The organic layer was dried (Na_2SO_4), filtered, and concentrated under a reduced pressure to obtain the title compound as a colorless oil (7.02 g, 80%). This compound was used in the next step without purification. HPLC 98% (t_R = 13.1 min, CH_3OH in 0.1% TFA water 5−95% in 20 min); ^{1}H NMR (500 MHz, DMSO-d_6) δ 8.04 (s, 1H), 7.51 (s, 1H), 4.39 (m, 1H), 3.50 (s, 1H), 2.97 (m, 2H), 2.24 (m, 1H), 1.74 (m, 1H), 1.59−1.34 (m, 4H), 1.26−1.05 (m, 3H); HPLC−MS (ESI+): *m*/*z* 301.1 $(M + H)^+$.

*3-(4-Bromo-1H-Pyrazol-1-yl)-3-Cyclopentylpropanoic Acid (**9**).* This compound was prepared according to the reported method.[27] To a solution of **8** (7.02 g, 23.40 mol, 1.0 eq), in dioxane (140 mL), was added sodium hydroxide (2.81 g, 70.20 mol, 3.0 eq) in water (70 mL). The reaction mixture was stirred overnight at room temperature. The mixture was concentrated under a reduced pressure and water (100 mL) was added followed by 1 N HCl to adjust the pH to 3 or 4. The aqueous layer was extracted with EtOAc (3 × 150 mL), dried (Na_2SO_4) and filtered, and concentrated under a reduced pressure to obtain the title compound as a white solid (6.20 g, 95%). This compound was used in the next step without further purification. HPLC 99% (t_R = 12.3 min, CH_3OH in 0.1% TFA water 5−95% in 20 min); ^{1}H NMR (500 MHz, DMSO-d_6) δ 12.21 (s, 1H), 8.02 (s, 1H), 7.51 (s, 1H), 4.37 (m, 1H), 2.86 (m, 2H), 2.23 (m, 1H), 1.75 (m, 1H), 1.60−1.35 (m, 4H), 1.26−1.06 (m, 3H); HPLC−MS (ESI+): *m*/*z* 287.2 $(M + H)^+$.

*(4R)-4-Benzyl-3-((3R)-3-(4-Bromo-1H-Pyrazol-1-yl)-3-Cyclopentylpropanoyl)Oxazolidin-2-One (4R,3R)-**10**.* To a solution of **9** (5.73 g, 20.0 mol, 1.0 eq) in tetrahydrofuran (172 mL), pivaloyl chloride (4.93 mL, 40.0 mol, 2.0 eq) and triethylamine (8.34 mL, 60.0 mol, 3.0 eq) were added at 0 °C. The reaction mixture was stirred for 1 h at room temperature. To the reaction mixture, lithium chloride (1.70 g, 40.0 mol, 2.0 eq) and oxazolidinone (3.58 g, 20.0 mol, 1.0 eq) were added, and then the mixture was stirred overnight at room temperature. The reaction mixture was diluted with water (100 mL), evaporated under a reduced pressure to remove tetrahydrofuran, and extracted with EtOAc (3 × 150 mL). The organic layer was evaporated under a reduced pressure and the residue was purified by SiO_2 chromatography using EtOAc/hexane (20%) as an eluent to give the title compound as a white solid (3.9 g, 42%, TLC: R_f = 0.51 developed using EtOAc/hexane (2:3)). HPLC 97% (t_R = 13.40 min, CH_3OH in 0.1% TFA water 5−95% in 20 min); ^{1}H NMR (500 MHz, DMSO-d_6) δ 8.10 (d, *J* = 0.7 Hz, 1H), 7.61 (s, 1H), 7.27−7.21 (m, 3H), 6.94−6.91 (m, 2H), 4.63−4.52 (m, 3H), 4.32 (t, *J* = 8.7 Hz, 1H), 4.17 (dd, *J* = 9.0, 3.1 Hz, 1H), 3.79 (dd, *J* = 17.6, 10.6 Hz, 1H), 3.20 (dd, *J* = 17.6, 2.9 Hz, 1H), 2.83−2.74 (m, 2H), 2.37−2.30 (m, 1H), 1.79−1.74 (m, 1H), 1.60−1.50 (m, 3H), 1.47−1.39 (m, 1H), 1.29−1.12 (m, 3H); HPLC−MS (ESI+): *m*/*z* 468.2 $(M + Na)^+$.

*(4R)-4-Benzyl-3-((3S)-3-(4-Bromo-1H-Pyrazol-1-yl)-3-Cyclopentylpropanoyl)Oxazolidin-2-One (4R,3S-**10**).* (**4R,3S**)-**10** was purified using the procedure described for (4*R*,3*R*)-**10** to obtain the title product as a white solid (4.0 g, 43%, TLC: R_f = 0.62 developed using EtOAc/hexane (2:3)). HPLC 98% (t_R = 13.60 min, CH_3OH in 0.1% TFA water 5−95% in 20 min); ^{1}H NMR (500 MHz, DMSO-d_6) δ 8.10 (d, *J* = 0.8 Hz, 1H), 7.52 (d, *J* = 0.6 Hz, 1H), 7.34−7.30 (m, 2H), 7.28−7.24 (m, 1H), 7.22−7.19 (m, 2H), 4.61−4.49 (m, 2H), 4.28 (t, *J* = 8.5 Hz, 1H), 4.15 (dd, *J* = 8.8, 2.8 Hz, 1H), 3.53 (dd, *J* = 17.1, 10.4 Hz, 1H), 3.37 (dd, *J* = 17.1, 3.0 Hz, 1H), 2.97 (dd, *J* = 13.6, 3.2 Hz, 1H), 2.84 (dd, *J* = 13.5, 8.3 Hz, 1H), 2.34−3.31 (m, 1H), 1.82−1.73 (m, 1H), 1.64−1.50 (m, 3H), 1.47−1.41 (m, 1H), 1.36−1.12 (m, 1H); HPLC−MS (ESI+): *m*/*z* 446.2 $(M + H)^+$.

*(S)-3-(4-Bromo-1H-Pyrazol-1-yl)-3-Cyclopentylpropanamide (**11**).* The amide **11** was synthesized using the same procedure described for **17** from (4*R*,3*S*)-**10** (7.6 mmol, 3.4 g) as a white solid (1.9 g, 87%). HPLC 97.2% (t_R = 11.4 min, CH_3OH in 0.1% TFA water 5−95% in 20 min); ^{1}H NMR (500 MHz, DMSO-d_6) δ 7.92 (s, 1H), 7.51 (s, 1H), 7.30 (s, 1H), 6.76 (s, 1H), 4.41 (td, *J* = 9.7, 4.1 Hz, 1H), 2.76 (dd, *J* = 15.3, 10.0 Hz, 1H), 2.57 (dd, *J* = 15.3, 4.0 Hz, 1H), 2.24 (h, *J* = 8.6 Hz, 1H), 1.79−1.70 (m, 1H), 1.59−1.35 (m, 4H), 1.24−1.06 (m, 3H); HPLC−MS (ESI+): *m*/*z* 286.2 $(M + H)^+$.

*(S)-3-(4-Bromo-1H-Pyrazol-1-yl)-3-Cyclopentylpropanenitrile (**12**).* The nitrile **12** was synthesized using the same procedure described for **18** from amide **11** (6.6 mmol, 1.9 g) as a white solid (1.6 g, 94%). HPLC 97.2% (t_R = 12.5 min, CH_3OH in 0.1% TFA water 5−95% in 20 min); ^{1}H NMR (500 MHz, DMSO-d_6) δ 8.13 (d, *J* = 0.7 Hz, 1H), 7.63 (s, 1H), 4.38 (td, *J* = 9.4, 4.7 Hz, 1H), 3.15−3.05 (m, 2H), 2.36−2.26 (m, 1H), 1.80−1.69 (m, 2H), 1.62−1.37 (m, 4H), 1.30−1.19 (m, 2H), 1.08 (dq, *J* = 12.7, 8.3 Hz, 1H); HPLC−MS (ESI+): *m*/*z* 268.0 $(M + H)^+$.

*(S)-3-Cyclopentyl-3-(4-(4,4,5,5-Tetramethyl-1,3,2-Dioxaborolan-2-yl)-1H-Pyrazol-1-yl)Propanenitrile (**13**).* The boronic ester **13** was synthesized using the same procedure described for **13** from (*S*)-bromopyrazole **19** (1.1 mmol, 0.3 g) as a white solid (165 mg, 47%). ^{1}H NMR (500 MHz, DMSO-d_6) δ 8.08 (s, 1H), 7.95 (s, 1H), 4.43 (td, *J* = 9.7, 4.3 Hz, 1H), 3.15−3.09 (m, 2H), 2.37−2.27 (m, 1H), 1.80−1.71 (m, 1H), 1.58−1.37 (m, 4H), 1.25 (s, 12H), 1.20−1.15 (m, 3H).

(S)-3-(4-(7H-Pyrrolo[2,3-d]Pyrimidin-4-yl)-1H-Pyrazol-1-yl)-3-Cyclopentylpropanenitrile [(S)-Ruxolitinib]. (*S*)-Ruxolitinib was synthesized using the same procedure described for **14** from (*S*)-**13** (0.15 mmol, 49 mg) as a white solid (35 mg, 74%). HPLC 99.17% (t_R = 12.57 min, CH_3OH 75% in 0.1% TFA water, 20 min); ^{1}H NMR (500 MHz, DMSO) δ 12.10 (s, 1H), 8.79 (s, 1H), 8.67 (s, 1H), 8.37 (s, 1H), 7.59 (dd, *J* = 3.5, 2.4 Hz, 1H), 6.98 (dd, *J* = 3.6, 1.7 Hz, 1H), 4.54 (td, *J* = 9.8, 4.0 Hz, 1H), 3.26 (dd, *J* = 17.2, 9.8 Hz, 2H), 2.42 (dd, *J* = 17.1, 8.3 Hz, 1H), 1.86−1.78 (m, 1H), 1.65−1.40 (m, 4H),

https://dx.doi.org/10.1021/acs.jmedchem.0c01952
J. Med. Chem. 2021, 64, 2228−2241

1.35−1.17 (m, 3H); HPLC−MS (ESI+): *m/z* 307.2 $(M+H)^+$. HRMS (ESI+) *m/z* calculated for $C_{17}H_{19}N_6$ $(M + H)^+$ 307.1666, found 307.1667.

(3RS)-3-(4-(7H-Pyrrolo[2,3-d]Pyrimidin-4-yl)-1H-Pyrazol-1-yl)-3-Cyclopentylpropanenitrile (rac-Ruxolitinib). To a solution of 4-bromo-7*H*-pyrrolo[2,3-*d*]pyrimidine (198 mg, 1.0 mmol, 1.0 eq), 3-cyclopentyl-3-(4-(4,4,5,5-tetramethyl-1,3,2-dioxaborolan-2-yl)-1H-pyrazol-1-yl)propanenitrile (378 mg, 1.2 mmol, 1.2 eq)[prepared from commercially available 4-(4,4,5,5-tetramethyl-1,3,2-dioxaborolan-2-yl)-1*H*-pyrazole and 3-cyclopentylprop-2-enenitrile according to a reported procedure],[32] and Na_2CO_3 (340 mg, 3.2 mmol, 3.2 eq) in dioxane (4 mL) and H_2O (1 mL) was added $Pd(PPh_3)_4$ (40 mg, 0.033 mmol, 0.033 eq). The pressure tube was purged with argon for 15 min, sealed, and then placed in a preheated oil bath at 120 °C. The mixture was stirred at this temperature for 12 h and then cooled to room temperature and partitioned between saturated NH_4Cl (20 mL) and EtOAc (10 mL). The layers were separated, and the aqueous layer was extracted twice more with EtOAc (10 mL). The combined organic extracts were washed with brine, dried ($MgSO_4$), and concentrated under a reduced pressure to give a yellow oil. Purification by flash chromatography (SiO_2, 75% EtOAc in hexane) provided the title compound *rac*-ruxolitinib as a brown powder (0.224 g, 73%). ^{1}H NMR (500 MHz, DMSO-d_6) δ: 12.11 (s, 1H), 8.80 (d, *J* = 0.7 Hz, 1H), 8.68 (s, 1H), 8.37 (s, 1H), 7.60 (dd, *J* = 3.6, 2.4 Hz, 1H), 6.99 (dd, *J* = 3.6, 1.8 Hz, 1H), 4.54 (td, *J* = 9.8, 4.1 Hz, 1H), 3.20 (m, 3H), 2.43 (m, 1H), 1.82 (m, 1H), 1.61 (m, 3H), 1.46 (m, 1H), 1.39 (m, 2H), 1.18 (m, 1H). HPLC−MS (ESI+): *m/z* 307.4 [100% $(M+H)^+$], HRMS (ESI+) *m/z* calculated for $C_{17}H_{19}N_6$ $(M + H)^+$ 307.1666, found 307.1662.

*(S)-3-(4-(2-Chloro-7H-Pyrrolo[2,3-d]Pyrimidin-4-yl)-1H-Pyrazol-1-yl)-3-Cyclopentylpropanenitrile (**14**).* The pyrrolopyrimidine **14** was synthesized using the same procedure described for **20** from (*S*)-boronic ester **13** (1.1 mmol, 0.3 g) as a white oil (151 mg, 41%). HPLC 78.0% (t_R = 11.99 min, CH_3OH in 0.1% TFA water 5−95% in 20 min); ^{1}H NMR (500 MHz, DMSO-d_6) δ 12.32 (s, 1H), 8.84 (d, *J* = 0.7 Hz, 1H), 8.39 (s, 1H), 7.64 (dd, *J* = 3.6, 2.3 Hz, 1H), 7.05 (dd, *J* = 3.6, 1.8 Hz, 1H), 4.56 (td, *J* = 9.8, 4.1 Hz, 1H), 3.29−3.21 (m, 2H), 2.43 (q, *J* = 8.6 Hz, 1H), 1.82 (td, *J* = 11.9, 7.2 Hz, 1H), 1.66−1.41 (m, 4H), 1.33−1.23 (m, 3H); HPLC−MS (ESI+): *m/z* 341.2 $(M + H)^+$.

*tert-Butyl (S)-2-Chloro-4-(1-(2-Cyano-1-Cyclopentylethyl)-1H-Pyrazol-4-yl)-7H-Pyrrolo[2,3-d]Pyrimidine-7-Carboxylate (**15**).* The boc-protected pyrrolopyrimidine **15** was synthesized using the same procedure described for **21** from (*S*)-pyrrolopyrimidine **14** (0.27 mmol, 92 mg) as a white solid (70 mg, 68%). HPLC 95.8% (t_R = 13.6 min, CH_3OH in 0.1% TFA water 5−95% in 20 min); ^{1}H NMR (500 MHz, DMSO-d_6) δ 8.91 (d, *J* = 0.7 Hz, 1H), 8.44 (s, 1H), 7.92 (d, *J* = 4.1 Hz, 1H), 7.27 (d, *J* = 4.2 Hz, 1H), 4.56 (td, *J* = 9.7, 4.1 Hz, 1H), 3.29−3.21 (m, 2H), 2.43 (q, *J* = 8.6 Hz, 1H), 1.82 (td, *J* = 12.2, 7.4 Hz, 1H), 1.64 (s, 8H), 1.58−1.41 (m, 4H), 1.35−1.23 (m, 3H); HPLC−MS (ESI+): *m/z* 441.2 $(M + H)^+$.

*tert-Butyl (S)-2-((4-(1-(tert-Butoxycarbonyl)Piperidin-4-yl)-Phenyl)Amino)-4-(1-(2-Cyano-1-Cyclopentylethyl)-1H-Pyrazol-4-yl)-7H-Pyrrolo[2,3-d]Pyrimidine-7-Carboxylate (**16**).* The *bis*-boc-protected pyrrolopyrimidine **16** was synthesized using the same procedure described for **22** from the (*S*)-pyrrolopyrimidine derivative **15** (0.09 mmol, 60 mg) as a yellow solid (47 mg, 76%). HPLC 97.0% (t_R = 15.04 min, CH_3OH in 0.1% TFA water 5−95% in 20 min); ^{1}H NMR (500 MHz, DMSO-d_6) δ 10.85 (s, 1H), 9.43 (s, 2H), 8.75 (d, *J* = 0.8 Hz, 1H), 8.33 (s, 1H), 7.92 (d, *J* = 8.6 Hz, 2H), 7.56 (d, *J* = 4.1 Hz, 1H), 7.15 (d, *J* = 8.5 Hz, 2H), 7.04 (d, *J* = 4.2 Hz, 1H), 4.56 (td, *J* = 9.6, 4.4 Hz, 2H), 3.26−3.21 (m, 2H), 2.65−2.62 (m, 1H), 2.45−2.40 (m, 1H), 1.85−1.80 (m, 1H), 1.76 (d, *J* = 13.1 Hz, 2H), 1.66−1.52 (m, 15H), 1.43 (s, 9H), 1.36−1.26 (m, 5H); HPLC−MS (ESI+): *m/z* 681.4 $(M + H)^+$.

*(S)-3-Cyclopentyl-3-(4-(2-((4-(Piperidin-4-yl)Phenyl)Amino)-7H-Pyrrolo[2,3-d]Pyrimidin-4-yl)-1H-Pyrazol-1-yl)Propanenitrile [**(S)-1**].* The anilinopiperidine (**S**)-**1** was synthesized using the same procedure described for (**R**)-**1** from (*S*)-pyrrolopyrimidine **16** (0.06 mmol, 42 mg) as a yellow solid (24 mg, 83%). HPLC 97.6% (t_R = 7.76 min, CH_3OH 50% and water 50% in 20 min); ^{1}H NMR (500 MHz, DMSO-d_6) δ 11.49 (s, 1H), 9.04 (s, 1H), 8.69 (s, 1H), 8.30 (s, 1H), 7.82−7.78 (m, 2H), 7.22 (dd, *J* = 3.7, 2.1 Hz, 1H), 7.15−7.11 (m, 2H), 6.79 (dd, *J* = 3.6, 1.6 Hz, 1H), 4.57 (td, *J* = 9.7, 4.2 Hz, 1H), 3.26−3.20 (m, 2H), 3.08 (d, *J* = 11.9 Hz, 2H), 2.68−2.61 (m, 2H), 1.87−1.80 (m, 1H), 1.73 (d, *J* = 12.6 Hz, 2H), 1.65−1.42 (m, 7H), 1.38−1.20 (m, 6H); HPLC−MS (ESI+): *m/z* 481.5 $(M+H)^+$. HRMS (ESI+) *m/z* calculated for $C_{28}H_{33}N_8$ $(M + H)^+$ 481.2823, found 481.2830.

*(R)-3-(4-Bromo-1H-Pyrazol-1-yl)-3-Cyclopentylpropanamide (**17**).* To a solution of (4*R*,3*R*)-**10** (3.0 g, 6.7 mol, 1.0 eq) in tetrahydrofuran (180 mL) was added ammonium hydroxide (30%, 120 mL). The reaction mixture was stirred for 2 days at room temperature. The mixture was diluted with methanol (250 mL), concentrated under a reduced pressure, and this process was repeated another two times. The residue obtained was purified by reverse-phase chromatography over a C-18 silica gel using methanol/dichloromethane (gradient elution 0 to 5%) as an eluent to give the title compound as a white solid (1.24 g, 64%). HPLC 95% (t_R = 11.44 min, CH_3OH in 0.1% TFA water 5−95% in 20 min); ^{1}H NMR (500 MHz, DMSO-d_6) δ 7.92 (d, *J* = 0.7 Hz, 1H), 7.51 (d, *J* = 0.7 Hz, 1H), 7.29 (s, 1H), 6.75 (s, 1H), 4.41 (td, *J* = 9.7, 4.0 Hz, 1H), 2.79−2.57 (m, 1H), 2.27−2.20 (m, 1H), 1.78−1.72 (m, 1H), 1.60−1.36 (m, 4H), 1.24−1.04 (m, 3H); HPLC−MS (ESI+): *m/z* 286.1 $(M + H)^+$.

*(R)-3-(4-Bromo-1H-Pyrazol-1-yl)-3-Cyclopentylpropanenitrile (**18**).* This compound was prepared according to the reported method.[27] To a solution of **17** (1.24 g, 4.3 mol, 1.0 eq), in tetrahydrofuran (50 mL), was added phosphorus pentoxide (1.84 g, 13.0 mol, 3 eq) under argon. The reaction mixture was stirred for 2 h at 70 °C, diluted with EtOAc (200 mL), and quenched by adding saturated sodium bicarbonate (200 mL). The aqueous layer was back-extracted with EtOAc (2 × 100 mL). The organic phases were combined, washed with water, brine, dried over anhydrous Na_2SO_4, and filtered. The filtrate was concentrated under a reduced pressure and purified by SiO_2 chromatography using methanol/dichloromethane (5%) as an eluent to provide the title compound as a white solid (1.13 g, 98%). HPLC 100% (t_R = 12.56 min, CH_3OH in 0.1% TFA water 5−95% in 20 min); ^{1}H NMR (500 MHz, DMSO-d_6) δ 8.12 (d, *J* = 0.5 Hz, 1H), 7.63 (d, *J* = 0.5 Hz, 1H), 4.38 (td, *J* = 9.4, 4.7 Hz, 1H), 3.15−3.08 (m, 2H), 2.33−2.28 (m, 1H), 1.79−1.72 (m, 1H), 1.61−1.38 (m, 4H), 1.30−1.05 (m, 3H); HPLC−MS (ESI+): *m/z* 268.0 $(M + H)^+$.

*(R)-3-Cyclopentyl-3-(4-(4,4,5,5-Tetramethyl-1,3,2-Dioxaborolan-2-yl)-1H-Pyrazol-1-yl)Propanenitrile (**19**).* This compound was prepared according to the reported method.[27] To a 20 mL microwave vial, **18** (0.30 g, 1.12 mmol, 1.0 eq), 4,4,5,5-tetramethyl-2-(4,4,5,5-tetramethyl-1,3,2-dioxaborolan-2-yl)-1,3,2-dioxaborolane (0.30 g, 1.19 mmol, 1.1 eq), potassium acetate (329 mg, 3.36 mmol, 3.0 eq), and 1,4-dioxane (4.0 mL) were added. The resulting reaction mixture was degassed by bubbling argon for 5 min before being treated with tetrakis(triphenylphosphine)palladium(0) (65 mg, 0.06 mmol, 0.05 eq). The resulting reaction mixture was heated to 120 °C in a microwave reactor for 2 h. The reaction mixture was filtered through a celite bed, and the celite bed was washed with dichloromethane and the organic layer was diluted with water (10 mL). The aqueous layer was extracted with dichloromethane (2 × 10 mL). The combined organic layers were concentrated under a reduced pressure, and the crude product was purified using SiO_2 chromatography (EtOAc 0−30% in hexane) to yield the title compound as a yellow oil (153 mg, 43%). ^{1}H NMR (500 MHz, DMSO-d_6) δ 8.09 (d, *J* = 0.7 Hz, 1H), 7.66 (d, *J* = 0.7 Hz, 1H), 4.43 (td, *J* = 9.6, 4.3 Hz, 1H), 3.19−3.05 (m, 2H), 2.33−2.31 (mz, 1H), 1.80−1.73 (m, 1H), 1.61−1.39 (m, 4H), 1.27 (s, 12H), 1.20−1.15 (m, 3H).

*(R)-3-(4-(2-Chloro-7H-Pyrrolo[2,3-d]Pyrimidin-4-yl)-1H-Pyrazol-1-yl)-3-Cyclopentylpropanenitrile (**20**).* To a 50 mL round-bottom flask were added 2,4-dichloro-7*H*-pyrrolo[2,3-*d*]pyrimidine (87.0 mg, 0.46 mmol, 0.95 eq), **19** (153.0 mg, 0.49 mmol, 1 eq), sodium carbonate (191 mg, 1.38 mmol, 3 eq), water (0.5 mL), and 1,4-dioxane (2.0 mL), and the resulting reaction mixture was degassed by bubbling argon for 5 min before adding $Pd(PPh_3)_4$ (17 mg, 0.01

https://dx.doi.org/10.1021/acs.jmedchem.0c01952
J. Med. Chem. 2021, 64, 2228−2241

mmol, 0.03 eq). The resulting reaction mixture was heated to 100 °C under argon overnight. The reaction mixture was gradually cooled down to ambient temperature and filtered through a celite bed. The celite bed was washed with dichloromethane (10 mL) and the organic layer was diluted with water (10 mL). The aqueous layer was extracted with dichloromethane (2 × 10 mL). The combined organic layers were concentrated under a reduced pressure to remove solvents, and the crude product was purified by SiO_2 chromatography (EtOAc 0−60% in hexane) to yield the title compound as a yellow solid (94 mg, 68%). HPLC 74.7% (t_R = 11.93 min, CH_3OH in 0.1% TFA water 5%∼95% in 20 min); ^{1}H NMR (600 MHz, DMSO-d_6) δ 12.32 (s, 1H), 8.84 (d, J = 0.8 Hz, 1H), 8.39 (s, 1H), 7.64 (d, J = 3.6, 1H), 7.05 (d, J = 3.6, 1H), 4.56 (td, J = 9.8, 4.0 Hz, 1H), 3.27−3.18 (m, 2H), 2.45−2.38 (m, 1H), 1.86−1.78 (m, 1H), 1.64−1.44 (m, 4H), 1.35−1.24 (m, 3H); HPLC−MS (ESI+): m/z 341.2 $(M + H)^+$.

*tert-Butyl (R)-2-Chloro-4-(1-(2-Cyano-1-Cyclopentylethyl)-1H-Pyrazol-4-yl)-7H-Pyrrolo[2,3-d]Pyrimidine-7-Carboxylate (**21**).* To a solution of pyrrolopyrimidine **20** (94.0 mg, 0.28 mmol, 1.0 eq), in dichloromethane (2.0 mL), *N*,*N*-diisopropylethylamine (0.058 mL, 0.33 mmol, 1.2 eq) was added and then di-*tert*-butyl dicarbonate (90.3 mg, 0.41 mmol, 1.5 eq) and 4-dimethylaminopyridine (7.0 mg, 0.06 mmol, 0.2 eq) were added. The reaction mixture was stirred for 2 h at room temperature. The reaction mixture was diluted with water (10 mL) and extracted with dichloromethane (3 × 10 mL). The organic phase was evaporated under a reduced pressure and the residue was purified by SiO_2 chromatography using EtOAc/hexane (50%) as an eluent to give the title compound as a white solid (98 mg, 80%). HPLC 95.2% (t_R = 13.63 min, CH_3OH in 0.1% TFA water 5%∼95% in 20 min); ^{1}H NMR (600 MHz, DMSO-d_6) δ 8.90 (d, J = 0.8 Hz, 1H), 8.43 (s, 1H), 7.91 (d, J = 4.1 Hz, 1H), 7.26 (d, J = 4.2 Hz, 1H), 4.55 (td, J = 9.8, 4.0 Hz, 1H), 3.24−3.16 (m, 2H), 1.85−1.78 (m, 1H), 1.58−1.40 (m, 4H), 1.35−1.22 (m, 12H); HPLC−MS (ESI+): m/z 441.2 $(M + H)^+$.

*tert-Butyl (R)-2-((4-(1-(tert-Butoxycarbonyl)Piperidin-4-yl)-Phenyl)Amino)-4-(1-(2-Cyano-1-Cyclopentylethyl)-1H-Pyrazol-4-yl)-7H-Pyrrolo[2,3-d]Pyrimidine-7-Carboxylate (**22**).* A mixture of boc-pyrrolopyrimidine **21** (47.0 mg, 0.11 mmol, 1.0 eq), *tert*-butyl 4-(4-aminophenyl)piperidine-1-carboxylate (30.0 mg, 0.11 mmol, 1.0 eq), and potassium carbonate (30.0 mg, 2 mmol, 2.0 eq) in anhydrous *tert*-butyl alcohol (2 mL) was degassed by bubbling argon. To this mixture, 2-dicyclohexylphosphino-2′,4′,6′-triisopropylbiphenyl (10.0 mg, 0.021 mmol, 0.2 eq) and tris(dibenzylideneacetone)dipalladium (10.0 mg, 0.01 mmol, 0.1 eq) were added. The reaction was refluxed overnight and then allowed to cool to room temperature; water was added (10 mL) and the mixture was extracted with dichloromethane (3 × 10 mL). The combined organic extracts were washed with brine, dried (Na_2SO_4), and filtered, and the solvent was removed under a reduced pressure. The residue was purified by SiO_2 chromatography using EtOAc/hexane (50%) as an eluent to give the title compound as a yellow solid (54 mg, 89%). HPLC 97.1% (t_R = 15.13 min, CH_3OH in 0.1% TFA water 5%∼95% in 20 min); ^{1}H NMR (500 MHz, DMSO-d_6) δ 9.43 (s, 1H), 8.75 (d, J = 0.7 Hz, 1H), 8.33 (s, 1H), 7.93−7.90 (m, 2H), 7.56 (d, J = 4.2 Hz, 1H), 7.15 (d, J = 8.6 Hz, 2H), 7.04 (d, J = 4.2 Hz, 1H), 4.56 (td, J = 9.6, 4.3 Hz, 1H), 3.27−3.20 (m, 2H), 2.46−2.43 (m, 1H), 1.87−1.79 (m, 1H), 1.76 (d, J = 13.0 Hz, 2H), 1.66 (s, 9H), 1.57−1.45 (m, 6H), 1.43 (s, 9H), 1.37−1.16 (m, 8H); HPLC−MS (ESI+): m/z 681.5 $(M + H)^+$.

(R)-3-Cyclopentyl-3-(4-(2-((4-(Piperidin-4-yl)Phenyl)Amino)-7H-Pyrrolo[2,3-d]Pyrimidin-4-yl)-1H-Pyrazol-1-yl)Propanenitrile [(R)-1)]. The *bis*-boc-protected derivative **16** (54.0 mg, 0.08 mmol, 1.0 eq) was suspended in dichloromethane (2 mL) and TFA (0.12 mL, 1.59 mmol, 20.0 eq) was added. The mixture was stirred at room temperature for 2 h and concentrated under a reduced pressure. The residue was dissolved in chloroform and washed with 10% potassium carbonate (aq.). The aqueous layer was extracted with chloroform (3 × 10 mL) and the combined organic phase was dried (Na_2SO_4) and filtered. The filtrate was concentrated under a reduced pressure, and the product was dried under vacuum to afford the title compound as a white solid (47 mg, 95%). HPLC 98.7% (t_R = 11.00 min, CH_3OH in 0.1% TFA water 5−95% in 20 min); ^{1}H NMR (500 MHz, DMSO-d_6) δ 11.49 (s, 1H), 9.01 (s, 1H), 8.68 (s, 1H), 8.30 (s, 1H), 7.80−7.76 (m, 2H), 7.21 (d, J = 3.6 Hz, 1H), 7.14−7.10 (m, 2H), 6.78 (d, J = 3.6 Hz, 1H), 4.56 (td, J = 9.6, 4.1 Hz, 1H), 3.22−3.17 (m, 2H), 3.02 (d, J = 11.9 Hz, 1H), 2.44−2.42 (m, 1H), 1.81−1.85 (m, 1H), 1.68 (d, J = 13.0 Hz, 2H), 1.61−1.44 (m, 6H), 1.36−1.22 (m, 8H); HPLC−MS (ESI+): m/z 681.5 $(M+H)^+$. HRMS (ESI+) m/z calculated for $C_{28}H_{33}N_8$ $(M+H)^+$ 481.2823, found 481.2830.

*3-(4-(4,4,5,5-Tetramethyl-1,3,2-Dioxaborolan-2-yl)-1H-Pyrazol-1-yl)Propanenitrile (**27**).*[33] Using the reported method,[31] a 100 mL round-bottom flask was charged with 4-(4,4,5,5-tetramethyl-1,3,2-dioxaborolan-2-yl)-1*H*-pyrazole (5.0 g, 25.8 mmol, 1.0 eq), acrylonitrile (1.04 g, 52.0 mmol, 2.0 eq), DBU (1.97 g, 12.9 mmol, 0.5 eq), and acetonitrile (50 mL). The mixture was stirred at room temperature overnight. After cooling, the mixture was diluted with EtOAc, washed with water twice and brine once, and dried over Na_2SO_4. After filtration, the filtrate was concentrated under a reduced pressure to yield the nitrile **27** as a yellow oil (3.9 g, 62%). ^{1}H NMR (500 MHz, DMSO-d_6) δ 8.04 (d, J = 0.6 Hz, 1H), 7.65 (d, J = 0.7 Hz, 1H), 4.41 (t, J = 6.4 Hz, 2H), 3.07 (t, J = 6.4 Hz, 2H), 1.26 (s, 9H).

*3-(4-(2-Chloro-7H-Pyrrolo[2,3-d]Pyrimidin-4-yl)-1H-Pyrazol-1-yl)Propanenitrile (**28**).* To a 50 mL round-bottom flask were added 2,4-dichloro-7*H*-pyrrolo[2,3-*d*]pyrimidine (3.0 g, 12.0 mmol, 1.2 eq), 3-(4-(4,4,5,5-tetramethyl-1,3,2-dioxaborolan-2-yl)-1*H*-pyrazol-1-yl)-propanenitrile **27** (0.51 g, 10.0 mmol, 1.0 eq), sodium carbonate (3.4 g, 31.6 mmol, 3.16 eq), water (H_2O, 13 mL), and 1,4-dioxane (53 mL), and the resulting reaction mixture was degassed by bubbling argon for 5 min before being treated with $Pd(PPh_3)_4$ (384 mg, 0.333 mmol). The resulting reaction mixture was heated to 100 °C under argon overnight. The reaction mixture was gradually cooled to ambient temperature before being filtered through a celite bed. The celite bed was washed with dichloromethane before the filtrate and washes were combined. The two layers were separated, and the aqueous layer was extracted with dichloromethane. The combined organic layers were concentrated under a reduced pressure to remove solvents, and the residue was purified by column chromatography (EtOAc 0 to 50% in hexane) to yield the title compound **28** as a brown solid (1.8 g, 69%). ^{1}H NMR (500 MHz, DMSO-d_6) δ 12.33 (s, 1H), 8.81 (d, J = 0.7 Hz, 1H), 8.37 (d, J = 0.7 Hz, 1H), 7.64 (dd, J = 3.6, 2.3 Hz, 1H), 7.03 (dd, J = 3.6, 1.7 Hz, 1H), 4.53 (t, J = 6.4 Hz, 2H), 3.19 (t, J = 6.4 Hz, 2H). HPLC−MS (ESI+): m/z 273.4 $(M+1)^+$, 567.3 $(2\ M+Na)^+$.

*tert-Butyl-2-Chloro-4-(1-(2-Cyanoethyl)-1H-Pyrazol-4-yl)-7H-Pyrrolo[2,3-d]Pyrimidine-7-Carboxylate (**29**).* To a solution of chloropyrrolopyrimidine **28** (850 mg, 3.12 mmol, 1.2 eq) in DCM (15 mL) were added $(Boc)_2O$ (1.0 g, 4.68 mmol, 1.5 eq), DIPEA (0.49 g, 3.75 mmol, 1.2 eq), and DMAP (76 mg, 0.624 mmol, 0.2 eq). The reaction mixture was stirred at room temperature for 12 h, quenched with water, and extracted with EtOAc (2 × 20 mL). The organic layer was dried (Na_2SO_4) and concentrated in vacuo to yield the title compound **29** as a brown solid (1.12 g, 96%). ^{1}H NMR (500 MHz, DMSO-d_6) δ 8.87 (d, J = 0.9 Hz, 1H), 8.40 (d, J = 0.7 Hz, 1H), 7.91 (d, J = 4.1 Hz, 1H), 7.25 (d, J = 4.2 Hz, 1H), 4.53 (t, J = 6.4 Hz, 2H), 3.19 (t, J = 6.4 Hz, 2H), 1.64 (s, 9H). HPLC−MS (ESI+): m/z 373.1 [60%, $(M+H)^+$], 769.2 [100% $(2M + Na)^+$].

*tert-Butyl-2-((4-(1-(tert-Butoxycarbonyl)Piperidin-4-yl)Phenyl)-Amino)-4-(1-(2-Cyanoethyl)-1H-Pyrazol-4-yl)-7H-Pyrrolo[2,3-d]-Pyrimidine-7-Carboxylate (**30**).* A mixture of *tert*-butyl-2-chloro-4-(1-(2-cyanoethyl)-1*H*-pyrazol-4-yl)-7*H*-pyrrolo[2,3-*d*]pyrimidine-7-carboxylate (**29**) (0.37 g, 1.0 mmol, 1.2 eq), *tert*-butyl-4-(4-aminophenyl)piperidine-1-carboxylate (0.33 g, 1.2 mmol, 1.2 eq), and K_2CO_3 (0.21 g, 1.5 mmol) in anhydrous ^{t}BuOH (10 mL) was degassed under argon. To this mixture were added XPhos (48 mg, 0.1 mmol) and $Pd_2(dba)_3$ (46 mg, 0.05 mmol) and the reaction mixture was heated for 6 h and then allowed to cool. Water (40 mL) was added and the mixture was extracted with CH_2Cl_2. The combined organic extracts were washed with brine, dried, and filtered, and the solvent was removed under a reduced pressure. The residue was purified by flash chromatography (50% EtOAc/hexane) to yield the title compound **30** as a brown solid (0.40 g, 79%). ^{1}H NMR (500 MHz, DMSO-d_6) δ 9.43 (s, 1H), 8.72 (d, J = 1.6 Hz, 1H), 8.31 (d, J =

https://dx.doi.org/10.1021/acs.jmedchem.0c01952
J. Med. Chem. 2021, 64, 2228−2241

1.5 Hz, 1H), 7.90 (d, J = 8.6 Hz, 1H), 7.55 (d, J = 4.2 Hz, 1H), 7.14 (d, J = 8.7 Hz, 2H), 7.01 (d, J = 4.2 Hz, 1H), 4.53 (m, 2H), 4.02 (m, 2H), 3.16 (m, 2H), 2.80 (m, 2H), 2.6 (m, 1H), 1.75 (m, 2H), 1.65 (s, 9H), 1.47 (m, 2H), 1.42 (s, 9H). HPLC−MS (ESI+): m/z 613.1 [100%, $(M + H)^+$].

3-(4-(2-((4-(Piperidin-4-yl)Phenyl)Amino)-7H-Pyrrolo[2,3-d]-Pyrimidin-4-yl)-1H-Pyrazol-1-yl)Propanenitrile (2). To a solution of the *bis*-boc-protected pyrrolopyrimidine **30** (0.306 g, 0.5 mmol) in DCM (3 mL) was added TFA (3 mL) under an argon atmosphere, and the reaction mixture was stirred at room temperature for 4 h. After this time, there was no starting material present (as measured by HPLC), and the reaction was quenched with sat. $NaHCO_3$ solution and extracted with DCM (2 × 10 mL). The combined organic layers were dried over Na_2SO_4 and evaporated to dryness in vacuo to yield the title compound **2** as a brown solid (0.121 g, 81%). ^{1}H NMR (500 MHz, DMSO-d_6) δ 11.49 (s, 1H), 9.06 (s, 1H), 8.67 (s, 1H), 8.29 (s, 1H), 7.80 (d, J = 8.3 Hz, 2H), 7.22 (d, J = 3.6 Hz, 1H), 7.13 (d, J = 8.3 Hz, 2H), 6.77 (d, J = 3.6 Hz, 1H), 4.53 (t, J = 6.4 Hz, 2H), 3.13 (m, 4H), 2.69 (m, 2H), 2.60 (m, 1H), 1.77 (dd, J = 13.6, 3.4 Hz, 2H), 1.58 (m, 2H). HPLC−MS (ESI+): m/z 207.2 [100% $(1/2\ M+H)^{2+}$], 413.3 [40% $(M + H)^+$]. m/z calculated for $C_{23}H_{25}N_8$ $(M+H)^+$ 413.2197, found 413.2191.

1-(But-3-en-1-yl)-4-(4,4,5,5-Tetramethyl-1,3,2-Dioxaborolan-2-yl)-1H-Pyrazole (31). A 100 mL round-bottom flask was charged with 4-(4,4,5,5-tetramethyl-1,3,2-dioxaborolan-2-yl)-1*H*-pyrazole (0.5 g, 2.58 mmol, 1.0 eq), 4-bromobutene (0.48 g, 3.6 mmol, 1.4 eq), cesium carbonate (1.67 g, 5.16 mmol, 2 eq), and acetonitrile (10 mL). The reaction mixture was stirred at 90 °C overnight. After cooling, the mixture was quenched with water (30 mL) and extracted with EtOAc (3 × 30 mL). The organic layers were combined, washed with brine (50 mL), dried (Na_2SO_4), and filtered. The solvent was evaporated under a reduced pressure to yield the title product as a yellow oil. ^{1}H NMR (500 MHz, chloroform-d) δ 7.78 (s, 1H), 7.67 (s, 1H), 5.78 (m, 1H), 5.09 (m, 2H), 4.20 (t, J = 7.5 Hz, 2H), 2.63 (m, 2H), 1.31 (s, 12H).

4-(1-(But-3-en-1-yl)-1H-Pyrazol-4-yl)-2-Chloro-7H-Pyrrolo[2,3-d]Pyrimidine (32). A 50 mL round-bottom flask was charged with 2,4-dichloro-7*H*-pyrrolo[2,3-*d*]pyrimidine (0.3 g, 1.6 mmol, 1.0 eq), 1-(but-3-en-1-yl)-4-(4,4,5,5-tetramethyl-1,3,2-dioxaborolan-2-yl)-1*H*-pyrazole **31** (0.51 g, 2.08 mmol, 1.5 eq), sodium carbonate (0.33 g, 3.2 mmol, 2.0 eq), water (H_2O, 5 mL), and 1,4-dioxane (15 mL). The reaction mixture was degassed by bubbling argon for 5 min before treating with $Pd(PPh_3)_4$ (199 mg, 0.172 mmol, 0.107 eq). The mixture was heated to 100 °C under argon overnight. The reaction mixture was gradually cooled down to ambient temperature, quenched with water (20 mL), and extracted with EtOAc (3 × 30 mL). The organic layers were combined, washed with brine (50 mL), dried (Na_2SO_4), and filtered. The solvent was evaporated under a reduced pressure, and the residue was triturated with Et_2O and hexane to give **32** as a yellow solid (0.32 g, 82%). ^{1}H NMR (500 MHz, DMSO-d_6) δ 12.28 (s, 1H), 8.69 (s, 1H), 8.28 (s, 1H), 7.60 (dd, J = 3.0, 1.5 Hz, 1H), 7.02 (d, J = 3.0 Hz, 1H), 5.84 (m, 1H), 5.08 (m, 2H), 4.31 (t, J = 7.5 Hz, 2H), 2.64 (m, 2H). HPLC−MS (ESI+): m/z 274.2 $(M+1)^+$, 569.2 $(2\ M + Na)^+$.

4-(1-(But-3-en-1-yl)-1H-Pyrazol-4-yl)-2-Chloro-7-Tosyl-7H-Pyrrolo[2,3-d]Pyrimidine (33). To a solution of 4-(1-(but-3-en-1-yl)-1*H*-pyrazol-4-yl)-2-chloro-7*H*-pyrrolo[2,3-*d*]pyrimidine **32** (1.0 g, 5.32 mmol, 1.0 eq), *p*-toluenesulfonyl chloride (1.1 g, 5.85 mmol, 1.1 eq), and tetra-butylammonium hydrogen sulfate (0.090 g, 0.27 mmol, 0.05 eq) in dichloromethane (20 mL) was added NaOH (50% aq, 0.2 mL). The reaction mixture was stirred at room temperature for 30 min. After completion of the reaction (as indicated by TLC), the reaction mixture was diluted with H_2O (20 mL). The organic layer was separated, washed with brine (50 mL), dried (Na_2SO_4), and filtered. The organic layer was evaporated under a reduced pressure to obtain a light yellow solid, which was purified by SiO_2 chromatography using hexane/EtOAc (5:1) as an eluent to give the title product (1.3 g, 85%). ^{1}H NMR (500 MHz, DMSO-d_6) δ 8.75 (s, 1H), 8.29 (s, 1H), 8.04 (d, J = 4.5 Hz, 1H), 8.03 (d, J = 8.5 Hz, 2H), 7.50 (d, J = 8.5 Hz, 2H), 7.37 (d, J = 4.5 Hz, 1H), 5.81 (m, 1H), 5.05 (m, 2H), 4.29 (t, J = 7.5 Hz, 2H), 2.61 (m, 2H). 2.37 (s, 3H). HPLC−MS (ESI+): m/z 428.1 $(M+1)^+$, 877.1 $(2M + Na)^+$.

tert-Butyl 4-(4-((4-(1-(But-3-en-1-yl)-1H-Pyrazol-4-yl)-7-Tosyl-7H-Pyrrolo[2,3-d]Pyrimidin-2-yl)Amino)Phenyl)Piperidine-1-Carboxylate (34). A mixture of 4-(1-(but-3-en-1-yl)-1H-pyrazol-4-yl)-2-chloro-7-tosyl-7H-pyrrolo[2,3-*d*]pyrimidine **33** (300 mg, 0.7 mmol, 1.0 eq), *tert*-butyl 4-(4-aminophenyl)piperidine-1-carboxylate (200 mg, 0.74 mmol, 1.06 eq), and K_2CO_3 (200 mg, 1.4 mmol, 2.0 eq) in anhydrous ^{t}BuOH (15 mL) was degassed by bubbling argon for 5 min. XPhos (33 mg, 0.07 mmol, 0.1 eq) and $Pd_2(dba)_3$ (32 mg, 0.035 mmol, 0.05 eq) were added and the mixture was refluxed overnight. The mixture was allowed to cool to room temperature and quenched with water (40 mL). The mixture was extracted with CH_2Cl_2 (3 × 30 mL). The combined organic extracts were washed with brine, dried (Na_2SO_4), and filtered, and the solvent was removed under a reduced pressure. The residue was purified by SiO_2 chromatography (0 to 60% EtOAc in hexane) to afford the title compound as a yellow solid (330 mg, 85%). ^{1}H NMR (500 MHz, DMSO-d_6) δ 9.52 (s, 1H), 8.60 (s, 1H), 8.19 (s, 1H), 8.02 (d, J = 8.0 Hz, 2H), 7.87 (d, J = 8.0 Hz, 2H), 7.70 (d, J = 4.0 Hz, 1H), 7.40 (d, J = 8.0 Hz, 2H), 7.24 (d, J = 8.0 Hz, 2H), 5.79 (m, 1H), 5.07 (m, 2H), 4.30 (t, J = 7.5 Hz, 2H), 4.09 (br s, 2H), 2.82 (br s, 2H), 2.69−2.58 (m, 4H), 2.32 (s, 3H), 1.80 (m, 2H), 1.53 (m, 2H), 1.48 (s, 9H). HPLC−MS (ESI+): m/z 668.3 $(M + 1)^+$.

tert-Butyl 4-(4-((4-(1-(but-3-en-1-yl)-1H-Pyrazol-4-yl)-7H-Pyrrolo[2,3-d]Pyrimidin-2-yl)Amino)Phenyl)Piperidine-1-Carboxylate (35). To a solution of *tert*-butyl 4-(4-((4-(1-(but-3-en-1-yl)-1*H*-pyrazol-4-yl)-7-tosyl-7*H*-pyrrolo[2,3-*d*]pyrimidin-2-yl)amino)-phenyl)piperidine-1-carboxylate **34** (165 mg, 0.29 mmol, 1.0 eq) in MeOH (5 mL) and H_2O (3 mL) was added K_2CO_3 (165 mg, 1.20 mmol, 4.0 eq) and the mixture was refluxed for 3 h. The mixture was diluted with H_2O (30 mL) and extracted with EtOAc (3 × 30 mL). The combined organic extracts were washed with brine, dried (Na_2SO_4), and filtered, and the solvent was removed under a reduced pressure to give a yellow residue. The residue was purified by SiO_2 flash chromatography (0 to 70% EtOAc in hexane) to give the title compound (105 mg, 87%) as a white solid. ^{1}H NMR (500 MHz, DMSO-d_6) δ 11.47 (s, 1H), 9.03 (s, 1H), 8.55 (s, 1H), 8.20 (s, 1H), 7.81 (d, J = 9.0 Hz, 2H), 7.19 (m, 1H), 7.14 (d, J = 9.0 Hz, 2H), 6.76 (m, 1H), 5.86 (m, 1H), 5.10 (m, 2H), 4.32 (t, J = 7.0 Hz, 2H), 4.10 (br s, 2H), 2.79 (br s, 2H), 2.65−2.58 (m, 3H), 1.76 (m, 2H), 1.49 (m, 2H), 1.42 (s, 9H). HPLC−MS (ESI+): m/z 514.4 $(M + 1)^+$.

4-(1-(But-3-en-1-yl)-1H-Pyrazol-4-yl)-N-(4-(Piperidin-4-yl)-Phenyl)-7H-Pyrrolo[2,3-d]Pyrimidin-2-Amine (3). *tert*-Butyl-4-(4-((4-(1-(but-3-en-1-yl)-1*H*-pyrazol-4-yl)-7*H*-pyrrolo[2,3-*d*]pyrimidin-2-yl)amino)phenyl)piperidine-1-carboxylate **35** (0.22 g, 0.43 mmol, 1.0 eq) was suspended in CH_2Cl_2 (2 mL) and TFA (0.65 mL, 8.5 mmol, 20 eq) was added. The mixture was stirred at room temperature for 2 h and concentrated under a reduced pressure. The residue was dissolved in $CHCl_3$ (20 mL) and washed with 10% K_2CO_3 (aq). The aqueous layer was extracted with $CHCl_3$ (3 × 20 mL). The organic layers were combined, dried (Na_2SO_4), and filtered. The filtrate was concentrated under a reduced pressure, and the residue was dried under vacuum to afford the title compound as an off-white solid (0.13 g, 75%). HPLC 99.8% (t_R = 8.90 min, CH_3OH 45% in H_2O (0.1% TFA), 1 mL/min, 20 min); ^{1}H NMR (500 MHz, DMSO-d_6) δ 11.47 (s, 1H), 9.00 (s, 1H), 8.55 (s, 1H), 8.20 (s, 1H), 7.79 (d, J = 7.5 Hz, 2H), 7.19 (d, J = 4 Hz, 1H), 7.12 (d, J = 7.5 Hz, 2H), 6.76 (d, J = 4 Hz, 1H), 5.86 (m, 1H), 5.10 (m, 2H), 4.32 (t, J = 7.0 Hz, 2H), 3.02 (br d, J = 12.0 Hz, 2H), 2.65 (q, J = 7 Hz, 2H), 2.59 (t, J = 12.5 Hz, 2H), 1.68 (d, J = 12.0 Hz, 2H), 1.53 (m, 2H); ^{13}C NMR (125 MHz, DMSO-d_6) δ 156.4, 154.2, 151.3, 140.0, 139.3, 139.1, 135.3, 131.3, 126.9, 123.6, 121.2, 118.7, 117.7, 107.6, 100.5, 51.3, 47.2, 42.4, 35.0, 34.3; HPLC−MS (ESI+): m/z 414.3 $(M + 1)^+$; HRMS (ESI+) m/z calculated for $C_{24}H_{28}N_7$ $(M + H)^+$ 414.2401, found 414.2402.

Dianilinopyrimidine Inhibitors of JAK2. *N*-(2-Fluoro-5-((2-((3-fluoro-4-(1-methylpiperidin-4-yl)phenyl)amino)-5-methylpyrimidin-4-yl)amino)phenyl)-2-methylpropane-2-sulfonamide (**4**)

This was prepared according the method reported.[34]

https://dx.doi.org/10.1021/acs.jmedchem.0c01952
J. Med. Chem. 2021, 64, 2228−2241

N-(5-((2-((3,5-Difluoro-4-(1-methylpiperidin-4-yl)phenyl)amino)-5-methylpyrimidin-4-yl)amino)-2-fluorophenyl)-2-methylpropane-2-sulfonamide (**5**)

This was prepared according the method reported.[34]

4-((4-((4-Chloro-3-((1,1-dimethylethyl)sulfonamido)phenyl)-amino)-5-methylpyrimidin-2-yl)amino)-2-fluoro-*N*-(1-methylpiperidin-4-yl)benzamide (**6**)

This was prepared according the method reported.[35]

N^4-(1-(*Tert*-Butylsulfonyl)indolin-6-yl)-N^2-(3-fluoro-4-(1-methylpiperidin-4-yl)phenyl)-5-methylpyrimidine-2,4-diamine (**7**)

This was prepared according the method reported.[34]

Cloning and Expression of JAK2 KD. The DNA of human JAK2 KD (JH1), encoding amino acids 840−1132, was synthesized and cloned into pcDNA 3.3 (GeneArt). The construct was expressed using a CMV promoter and contained a His_8 *N*-terminal affinity tag followed by a TEV cleavage site. Expi293F cells (Invitrogen) were grown, maintained, and treated in a shaking culture at 37 °C with 8% CO_2 in Expi293 medium (Invitrogen). Recombinant JAK2 was expressed in Expi293F cells using Transporter 5 transfection reagent as described by the manufacturer (Polysciences). One hour after adding the plasmid/transfection complex, varying concentrations of the JAK2 inhibitor or the transcription enhancer were added as indicated in Figure 1. The transfection proceeded for 24 h before harvest. Cells used for the preparation of crystallization-grade JAK2 were incubated with 1 μM ruxolitinib and 4 mM butyric acid for 23 h.

Purification of JAK2 KD. Purification of JAK2 KD was performed at 4 °C. Expi293F cells were centrifuged at 1000 × g for 30 min at 4 °C. Cells were resuspended in lysis buffer (50 mM HEPES pH 7.5, 250 mM NaCl, 10% glycerol, 5 mM β-mercaptoethanol, 5 mM $MgCl_2$, 0.1 mM ATP, 10 mM imidazole, 1 mM PMSF, and 0.5% Triton X-100). The cells were sonicated at 40% power for 2 min on ice and then centrifuged at 40,000 × g for 1 h at 4 °C to clarify the lysate. The soluble lysate was loaded onto two 5 mL HisTrap FF columns in tandem (GE Healthcare). The columns were washed with 10 mM imidazole, 40 mM imidazole, 100 mM imidazole, and 200 mM imidazole before applying a gradient up to 600 mM imidazole. The protein was concentrated to 10 mL using a 10,000 MWCO filter and loaded onto an S75 gel filtration column (GE Healthcare) that was pre-equilibrated with 40 mM bicine pH 8.6, 100 mM NaCl, and 10% glycerol. The single JAK2 peak, as determined by sodium dodecyl sulfate−polyacrylamide gel electrophoresis (SDS-PAGE) and western blot analysis (>99% purity), was collected, concentrated to 8.1 mg/mL using a 3000 MWCO spin concentrator, flash-frozen in liquid N_2, and stored at −80 °C.

Cellular Thermal Shift Assay. CETSA was used to compare the melting curves from ligand-based thermal stabilization of JAK2 KD. Expi293F cells were transfected with His-JAK2 KD from pcDNA 3.3 as described above. Ruxolitinib (20 μM), or the equivalent amount of DMSO, was added to the cells and incubated for 1 h at 37 °C. After 1 h, the cells were centrifuged at 300 × g for 3 min at room temperature. The cells were washed with 15 mL of PBS and centrifuged again at 300 × g for 3 min. The cells were resuspended in 1 mL of PBS and approximately 3 × 10^6 cells were added to PCR tubes that were incubated at 40, 43, 46, 49, 52, 55, 58, 61, 64, or 67 °C for 3 min. The tubes were then flash-frozen in liquid N_2 and thawed twice at 25 °C. The cells were vortexed at 20,000 × g for 20 min at 4 °C. The soluble lysate was transferred to a new tube, a 5 × SDS-PAGE loading buffer was added, and 13 μL (equivalent of 3.3 × 10^5 cells) was added to an SDS-PAGE gel. The gel was transferred using the eBlot transfer system (GenScript), blocked with 5% BSA in TBS-T, and blotted for anti-His-HRP, anti-actin, or anti-GAPDH-HRP for 2 h at room temperature. The anti-actin blot was washed and then incubated with an anti-mouse-HRP-conjugated secondary antibody at 1:2000 for 1 h at room temperature. The blots were incubated with SignalFire ECL (Cell Signaling, 6883) and imaged using a GE Healthcare AmerSham Imager 600.

Isothermal Dose Response. ITDR measures protein stabilization as a function of increasing inhibitor concentration. After performing the CETSA assay described above, the data were graphed and a temperature at the IC_{50} value (47 °C) was used for the ITDR experiment. Expi293F cells were transfected with His-JAK2 KD. The cells were centrifuged at 300 × g for 3 min at room temperature. Cells were resuspended at a density of 4 × 10^7 cells/mL. Serial dilutions were performed yielding threefold dilutions ranging from 10 nM to 20 μM inhibitor with constant amounts of DMSO. Cells (approximately 1.2 × 10^6 cells) were added to the compounds and were incubated for 30 min at 37 °C with shaking every 10 min. The tubes were heated at 47 °C for 3 min. The cells were then vitrified and thawed twice at 25 °C before being vortexed at 20,000 × g for 20 min at 4 °C. The soluble supernatant was transferred to a new tube, mixed with a 5 × SDS-loading dye, and resolved on SDS-PAGE. The western blot transfer and incubation are the same as described above. Data were normalized to 0% and 100%.

Cell Viability Assays. UKE-1 cells were cultured in RPMI-1640 with 10% FBS at 37 °C with 5% CO_2. Suspension cells were seeded at 20,000 cells per well. Cells were incubated with increasing concentrations of compound ranging from 1 nM to 10 μM (as denoted in the figure legends) in the presence of a vehicle (0.2% DMSO) with six replicates per concentration for 72 h at 37 °C. After drug treatment, 15 μL of CellTiter Blue (Promega) was added to each well, mixed for 1 min using an orbital shaker, and incubated at 37 °C for 3 h. Fluorescence was measured using a Wallac EnVision 2130 plate reader (PerkinElmer). Excitation and emission filters of 570 and 615 nm were used, respectively. The cell viability data were analyzed using GraphPad Prism6.

Protein Crystallography. Purified His-JAK2 KD at 8.1 mg/mL was incubated with 1 mM ruxolitinib and then added to 0.2 M NaCl, 0.1 M Bis−Tris pH 5.5, and 25% PEG 3350 in a 1:1 v/v ratio on a hanging drop coverslip with the crystallization solution at 293 K. Rodlike crystals were formed within 10 h and grew to a maximum size over 5 days. Ligand exchange was performed by moving JAK2−ruxolitinib crystals into the crystallization solution containing 1 mM inhibitor of interest for 3 days. The crystals were preserved in a cryoprotectant containing the crystallization solution and 30% glycerol. All data were collected on the 23-ID beamline, GM/CA at the Advanced Photon Source (Argonne, IL). Data were processed and scaled with XDS. Molecular replacement (using PDB 2XA4 as the search model) and refinements were carried out using PHENIX, and model building was performed using Coot. Figures were prepared using PyMOL (Schrödinger, LLC). All structures were validated and deposited in the PDB with accession codes listed in Supplementary Tables S1-S2.

PDB ID CODES

6VGL (JAK2/ruxolitinib), 6VSN (JAK2/S-ruxolitinib), 6VNK (JAK2/rac-ruxolitinib), 6VN8 (JAK2/baricitinib), 6VNC (JAK2/R-**1**), 6VNB (JAK2/S-**1**), 6VS3 (JAK2/rac-**1**), 6VNJ (JAK2/**2**), 6VNM (JAK2/**3**), 6VNE (JAK2/fedratinib), 6VNG (JAK2/**4**), 6VNH (JAK2/**5**), 6VNL (JAK2/**6**), and 6VNF (JAK2/**7**). Authors will release the atomic coordinates and structure factors upon article publication.

The authors declare no competing financial interest.

ASSOCIATED CONTENT

Supporting Information

The Supporting Information is available free of charge at https://pubs.acs.org/doi/10.1021/acs.jmedchem.0c01952.

Molecular formula strings (CSV)

Supplementary figures, schematics and tables (PDF)

AUTHOR INFORMATION

Corresponding Author

Ernst Schönbrunn − *Drug Discovery Department, Moffitt Cancer Center, Tampa, Florida 33612, United States;* orcid.org/0000-0002-3589-3510; Email: ernst.schonbrunn@moffitt.org

https://dx.doi.org/10.1021/acs.jmedchem.0c01952
J. Med. Chem. 2021, 64, 2228−2241

Authors

Ryan R. Davis − *Drug Discovery Department, Moffitt Cancer Center, Tampa, Florida 33612, United States*
Baoli Li − *Drug Discovery Department, Moffitt Cancer Center, Tampa, Florida 33612, United States*
Sang Y. Yun − *Chemical Biology Core, Moffitt Cancer Center, Tampa, Florida 33612, United States*
Alice Chan − *Drug Discovery Department, Moffitt Cancer Center, Tampa, Florida 33612, United States*
Pradeep Nareddy − *Drug Discovery Department, Moffitt Cancer Center, Tampa, Florida 33612, United States*
Steven Gunawan − *Drug Discovery Department, Moffitt Cancer Center, Tampa, Florida 33612, United States*
Muhammad Ayaz − *Chemical Biology Core, Moffitt Cancer Center, Tampa, Florida 33612, United States*
Harshani R. Lawrence − *Chemical Biology Core, Moffitt Cancer Center, Tampa, Florida 33612, United States;* orcid.org/0000-0002-9263-7775
Gary W. Reuther − *Molecular Oncology Department, Moffitt Cancer Center, Tampa, Florida 33612, United States*
Nicholas J. Lawrence − *Drug Discovery Department, Moffitt Cancer Center, Tampa, Florida 33612, United States*

Complete contact information is available at: https://pubs.acs.org/10.1021/acs.jmedchem.0c01952

Notes

The authors declare no competing financial interest.

■ ACKNOWLEDGMENTS

We thank the GM/CA station at the Argonne National Laboratory for assistance with synchrotron data collection (National Cancer Institute grant Y1-CO-1020, National Institute of General Medical Sciences grant Y1-GM-1104, and U.S. Department of Energy contract W-31-109-ENG-38). We thank the Moffitt Chemical Biology Core for use of the crystallization and crystallography facility, and NMR and mass spectrometry instruments (National Cancer Institute grant P30-CA076292). H.R.L. acknowledges support by the National Cancer Institute grant R50CA211447. This work was supported by the Leukemia & Lymphoma Society (Screen-to-lead grant 8012-18) and the Florida Department of Health (Bankhead−Coley grant 20B10).

■ ABBREVIATIONS

JAK2, Janus kinase 2; MPN, myeloproliferative neoplasms; KD, kinase domain; SAR, structure−activity relationship; STATs, signal transducer and activator of transcription proteins

■ REFERENCES

(1) Vogelstein, B.; Papadopoulos, N.; Velculescu, V. E.; Zhou, S.; Diaz, L. A., Jr.; Kinzler, K. W. Cancer genome landscapes. *Science* **2013**, *339*, 1546−1558.
(2) Hubbard, S. R. Mechanistic insights into regulation of JAK2 tyrosine kinase. *Front. Endocrinol. (Lausanne)* **2017**, *8*, 361.
(3) Kesarwani, M.; Huber, E.; Kincaid, Z.; Evelyn, C. R.; Biesiada, J.; Rance, M.; Thapa, M. B.; Shah, N. P.; Meller, J.; Zheng, Y.; Azam, M. Targeting substrate-site in Jak2 kinase prevents emergence of genetic resistance. *Sci. Rep.* **2015**, *5*, No. 14538.
(4) Koppikar, P.; Bhagwat, N.; Kilpivaara, O.; Manshouri, T.; Adli, M.; Hricik, T.; Liu, F.; Saunders, L. M.; Mullally, A.; Abdel-Wahab, O.; Leung, L.; Weinstein, A.; Marubayashi, S.; Goel, A.; Gonen, M.; Estrov, Z.; Ebert, B. L.; Chiosis, G.; Nimer, S. D.; Bernstein, B. E.; Verstovsek, S.; Levine, R. L. Heterodimeric JAK-STAT activation as a mechanism of persistence to JAK2 inhibitor therapy. *Nature* **2012**, *489*, 155−159.
(5) Gorantla, S. P.; Babu, K. S.; Illert, A. L.; von Bubnoff, N.; Peschel, C.; Duyster, J. Ruxolitinib mediated paradox JAK2 hyperphosphorylation is due to the protection of activation loop phosphotyrosines from phosphatases. *Blood* **2013**, *122*, No. 2847.
(6) Tvorogov, D.; Thomas, D.; Liau, N. P. D.; Dottore, M.; Barry, E. F.; Lathi, M.; Kan, W. L.; Hercus, T. R.; Stomski, F.; Hughes, T. P.; Tergaonkar, V.; Parker, M. W.; Ross, D. M.; Majeti, R.; Babon, J. J.; Lopez, A. F. Accumulation of JAK activation loop phosphorylation is linked to type I JAK inhibitor withdrawal syndrome in myelofibrosis. *Sci. Adv.* **2018**, *4*, No. eaat3834.
(7) Bandaranayake, R. M.; Ungureanu, D.; Shan, Y.; Shaw, D. E.; Silvennoinen, O.; Hubbard, S. R. Crystal structures of the JAK2 pseudokinase domain and the pathogenic mutant V617F. *Nat. Struct. Mol. Biol.* **2012**, *19*, 754−759.
(8) Meyer, S. C. Mechanisms of resistance to JAK2 inhibitors in myeloproliferative neoplasms. *Hematol. Oncol. Clin. North Am.* **2017**, *31*, 627−642.
(9) Bousoik, E.; Montazeri Aliabadi, H. Do we know jack about JAK? A closer look at JAK/STAT signaling pathway. *Front. Oncol.* **2018**, *8*, No. 287.
(10) Karantanos, T.; Moliterno, A. R. The roles of JAK2 in DNA damage and repair in the myeloproliferative neoplasms: Opportunities for targeted therapy. *Blood Rev.* **2018**, *32*, 426−432.
(11) Schieber, M.; Crispino, J. D.; Stein, B. Myelofibrosis in 2019: moving beyond JAK2 inhibition. *Blood Cancer J.* **2019**, *9*, 74.
(12) Tefferi, A. JAK inhibitors for myeloproliferative neoplasms: clarifying facts from myths. *Blood* **2012**, *119*, 2721−2730.
(13) Quintas-Cardama, A.; Vaddi, K.; Liu, P.; Manshouri, T.; Li, J.; Scherle, P. A.; Caulder, E.; Wen, X.; Li, Y.; Waeltz, P.; Rupar, M.; Burn, T.; Lo, Y.; Kelley, J.; Covington, M.; Shepard, S.; Rodgers, J. D.; Haley, P.; Kantarjian, H.; Fridman, J. S.; Verstovsek, S. Preclinical characterization of the selective JAK1/2 inhibitor INCB018424: therapeutic implications for the treatment of myeloproliferative neoplasms. *Blood* **2010**, *115*, 3109−3117.
(14) Caruso, C. Fedratinib becomes new option in myelofibrosis. *Cancer Discov.* **2019**, *9*, 1332.
(15) Mullard, A. FDA approves Eli Lilly's baricitinib. *Nat. Rev. Drug Discov.* **2018**, *17*, 460.
(16) Zhou, T.; Georgeon, S.; Moser, R.; Moore, D. J.; Caflisch, A.; Hantschel, O. Specificity and mechanism-of-action of the JAK2 tyrosine kinase inhibitors ruxolitinib and SAR302503 (TG101348). *Leukemia* **2014**, *28*, 404−407.
(17) Lamontanara, A. J.; Gencer, E. B.; Kuzyk, O.; Hantschel, O. Mechanisms of resistance to BCR-ABL and other kinase inhibitors. *Biochim. Biophys. Acta* **2013**, *1834*, 1449−1459.
(18) Jafari, R.; Almqvist, H.; Axelsson, H.; Ignatushchenko, M.; Lundback, T.; Nordlund, P.; Martinez Molina, D. The cellular thermal shift assay for evaluating drug target interactions in cells. *Nat. Protoc.* **2014**, *9*, 2100−2122.
(19) Ember, S. W.; Lambert, Q. T.; Berndt, N.; Gunawan, S.; Ayaz, M.; Tauro, M.; Zhu, J. Y.; Cranfill, P. J.; Greninger, P.; Lynch, C. C.; Benes, C. H.; Lawrence, H. R.; Reuther, G. W.; Lawrence, N. J.; Schonbrunn, E. Potent dual BET bromodomain-kinase inhibitors as value-added multitargeted chemical probes and cancer therapeutics. *Mol. Cancer Ther.* **2017**, *16*, 1054−1067.
(20) Quentmeier, H.; MacLeod, R. A.; Zaborski, M.; Drexler, H. G. JAK2 V617F tyrosine kinase mutation in cell lines derived from myeloproliferative disorders. *Leukemia* **2006**, *20*, 471−476.
(21) Duan, Y.; Chen, L.; Chen, Y.; Fan, X. G. c-Src binds to the cancer drug Ruxolitinib with an active conformation. *PLoS One* **2014**, *9*, No. e106225.
(22) Williams, N. K.; Bamert, R. S.; Patel, O.; Wang, C.; Walden, P. M.; Wilks, A. F.; Fantino, E.; Rossjohn, J.; Lucet, I. S. Dissecting specificity in the Janus kinases: the structures of JAK-specific inhibitors complexed to the JAK1 and JAK2 protein tyrosine kinase domains. *J. Mol. Biol.* **2009**, *387*, 219−232.

(23) Hall, T.; Emmons, T. L.; Chrencik, J. E.; Gormley, J. A.; Weinberg, R. A.; Leone, J. W.; Hirsch, J. L.; Saabye, M. J.; Schindler, J. F.; Day, J. E.; Williams, J. M.; Kiefer, J. R.; Lightle, S. A.; Harris, M. S.; Guru, S.; Fischer, H. D.; Tomasselli, A. G. Expression, purification, characterization and crystallization of non- and phosphorylated states of JAK2 and JAK3 kinase domain. *Protein Expression Purif.* **2010**, *69*, 54−63.
(24) Zimmermann, K.; Sang, X.; Mastalerz, H. A.; Johnson, W. L.; Zhang, G.; Liu, Q.; Batt, D.; Lombardo, L. J.; Vyas, D.; Trainor, G. L.; Tokarski, J. S.; Lorenzi, M. V.; You, D.; Gottardis, M. M.; Lippy, J.; Khan, J.; Sack, J. S.; Purandare, A. V. 9H-Carbazole-1-carboxamides as potent and selective JAK2 inhibitors. *Bioorg. Med. Chem. Lett.* **2015**, *25*, 2809−2812.
(25) Vazquez, M. L.; Kaila, N.; Strohbach, J. W.; Trzupek, J. D.; Brown, M. F.; Flanagan, M. E.; Mitton-Fry, M. J.; Johnson, T. A.; TenBrink, R. E.; Arnold, E. P.; Basak, A.; Heasley, S. E.; Kwon, S.; Langille, J.; Parikh, M. D.; Griffin, S. H.; Casavant, J. M.; Duclos, B. A.; Fenwick, A. E.; Harris, T. M.; Han, S.; Caspers, N.; Dowty, M. E.; Yang, X.; Banker, M. E.; Hegen, M.; Symanowicz, P. T.; Li, L.; Wang, L.; Lin, T. H.; Jussif, J.; Clark, J. D.; Telliez, J. B.; Robinson, R. P.; Unwalla, R. Identification of N-{cis-3-[Methyl(7H-pyrrolo[2,3-d]-pyrimidin-4-yl)amino]cyclobutyl}propane-1-sulfo namide (PF-04965842): A selective JAK1 clinical candidate for the treatment of autoimmune diseases. *J. Med. Chem.* **2018**, *61*, 1130−1152.
(26) Zak, M.; Mendonca, R.; Balazs, M.; Barrett, K.; Bergeron, P.; Blair, W. S.; Chang, C.; Deshmukh, G.; Devoss, J.; Dragovich, P. S.; Eigenbrot, C.; Ghilardi, N.; Gibbons, P.; Gradl, S.; Hamman, C.; Hanan, E. J.; Harstad, E.; Hewitt, P. R.; Hurley, C. A.; Jin, T.; Johnson, A.; Johnson, T.; Kenny, J. R.; Koehler, M. F.; Bir Kohli, P.; Kulagowski, J. J.; Labadie, S.; Liao, J.; Liimatta, M.; Lin, Z.; Lupardus, P. J.; Maxey, R. J.; Murray, J. M.; Pulk, R.; Rodriguez, M.; Savage, S.; Shia, S.; Steffek, M.; Ubhayakar, S.; Ultsch, M.; van Abbema, A.; Ward, S. I.; Xiao, L.; Xiao, Y. Discovery and optimization of C-2 methyl imidazopyrrolopyridines as potent and orally bioavailable JAK1 inhibitors with selectivity over JAK2. *J. Med. Chem.* **2012**, *55*, 6176−6193.
(27) Cao, B.; Zhu, H.; Wu, J.; Tian, G. Intermediate of JAK inhibitor and preparation method thereof. *China patent* 2018, CN107759623A.
(28) Steele, A. D.; Keohane, C. E.; Knouse, K. W.; Rossiter, S. E.; Williams, S. J.; Wuest, W. M. Diverted total synthesis of promysalin analogs demonstrates that an iron-binding motif is responsible for its narrow-spectrum antibacterial activity. *J. Am. Chem. Soc.* **2016**, *138*, 5833−5836.
(29) Yao, L.; Mustafa, N.; Tan, E. C.; Poulsen, A.; Singh, P.; Duong-Thi, M. D.; Lee, J. X. T.; Ramanujulu, P. M.; Chng, W. J.; Yen, J. J. Y.; Ohlson, S.; Dymock, B. W. Design and synthesis of ligand efficient dual inhibitors of Janus kinase (JAK) and histone deacetylase (HDAC) based on ruxolitinib and vorinostat. *J. Med. Chem.* **2017**, *60*, 8336−8357.
(30) Yao, L.; Ramanujulu, P. M.; Poulsen, A.; Ohlson, S.; Dymock, B. W. Merging of ruxolitinib and vorinostat leads to highly potent inhibitors of JAK2 and histone deacetylase 6 (HDAC6). *Bioorg. Med. Chem. Lett.* **2018**, *28*, 2636−2640.
(31) Akri-Topoulou-Zanze, I.; Wakefield, B. D.; Mack, H.; Turner, S. C.; Gasiecki, A. F.; Gracias, V. J.; Sarris Kathy, A.; Kalvin, D. M.; Michmerhuizen, M. J.; Shuai, Q.; Patel, J. R.; Bakker, M.; Teusch, N.; Johnson, E. T.; Kovar, P. J.; Djuric, S. W.; Long, A. J.; Vasudevan, A.; George, D.; Wang, L.; Li, B.; St. John Moore, N.; Hobson, A. D.; Woods, K. W.; Miyashiro, J. M.; Swann, S. L. J.; Penning, T. D. 5-Substituted Indazoles as Kinase Inhibitors. US patent 2014, 8,648,069B2.
(32) Zhou, J.; Liu, P.; Lin, Q.; Metcalf, B. W.; Meloni, D.; Pan, Y.; Xia, M.; Li, M.; Yue, T.-Y.; Rodgers, J. D.; Wang, H. Processes for Preparing JAK Inhibitors and Related Compounds. US patent 2013, US8,410,265B2.
(33) Akri-Topoulou-Zanze, I.; Wakefield, B. D.; Mack, H.; Turner, S. C.; Gasiecki, A. F.; Gracias, V. J.; Kathy, S.; Kalvin, D. M.; Michmerhuizen, M. J.; Shuai, Q.; Patel, J. R.; Bakker, M.; Teusch, N.; Johnson, E. T.; Kovar, P. J.; Djuric, S. W.; Long, A. J.; Vasude-Van, A.; Hobson, A.; St. John Moore, N.; Wang, L.; George, D.; Li, B.; Frank, K. 5-Heteroaryl Substituted Indazoles as Kinase Inhibitors. PCT patent application 2013, WO2008/154241A1.
(34) Schonbrunn, E.; Lawrence, N. J.; Lawrence, H. R. BRD4-JAK2 Inhibitors. PCT patent application 2020, WO2020/051572.
(35) Schonbrunn, E.; Lawrence, N. J.; Lawrence, H. R. Potent Dual BRD4-Kinase Inhibitors as Cancer Therapeutics. *US patent* 2018, US10,106,507B2.

https://dx.doi.org/10.1021/acs.jmedchem.0c01952
J. Med. Chem. 2021, 64, 2228−2241